HHS Public Access

Author manuscript

Adv Biochem Eng Biotechnol. Author manuscript; available in PMC 2026 January 11.

Published in final edited form as:

Adv Biochem Eng Biotechnol. 2024 ; 187: 37–70. doi:10.1007/10_2024_252.

Applications of Graphene Field Effect Biosensors for Biological Sensing

Kiana Aran,

Shu Chien-Gene Lay Department of Bioengineering, Jacobs School of Engineering, University of California, San Diego, La Jolla, CA, USA

Division of Geriatrics, Gerontology and Palliative Care, Department of Medicine, School of Medicine, University of California, San Diego, La Jolla, CA, USA

Center for Technologies for Healthy Aging, Institute of Engineering and Medicine, University of California, San Diego, La Jolla, CA, USA

Paragraf, Somersham, UK

CRISPR QC, San Diego, CA, USA

Brett Goldsmith,

Paragraf, Somersham, UK

Maryam Moarefian

University of California, Santa Cruz, CA, USA

Abstract

This chapter provides a comprehensive overview of the principles, applications, and advancements in graphene field-effect transistor (gFET) biosensors for biological sensing. The unique properties of graphene that make it ideal for biosensing, including its high conductivity, chemical stability, and ability to facilitate label-free detection, will be discussed. The chapter also explores various applications of gFET biosensors, from detecting pH and salinity changes to complex protein-protein interactions and DNA/RNA sensing. It also addresses the challenges and future directions in gFET biosensor technology, emphasizing the need for scalable manufacturing, sophisticated surface chemistry, and the integration of multiomics approaches to enhance biosensing capabilities.

Graphical Abstract

✉ karan@ucsd.edu .

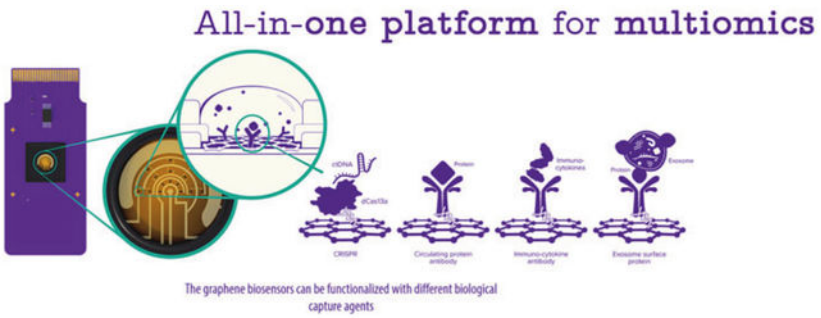

Keywords

CRISPR; Field effect Biosesnors; Mutiomics

1 Introduction and Background

Biomedical and environmental testing currently require access to highly specialized facilities or extensive training. Biochemical tests require complex reagents to achieve a simple human readable result such as a color change. Although we have already test systems for providing defined readout with affordable costs (e.g., glucose, virus detection, or pregnancy tests), there are still many high-cost tests with insufficient information about human diseases. To maximize information from testing while minimizing costs, biotechnology should leverage complex analysis enabled by advanced portable computing power and use simplified reagents, tools, and processes. This concept can be conceived of as “the internet of biology” in the same way miniaturized electronic sensors have enabled “the internet of things.” Nanotechnologists have created proof-of-concept hand-held, easy-to-use personal devices, but none have achieved large-scale manufacturability. We introduce here the concept, principle, and application of the first economical nanoelectronics produced in a commercial foundry. The mass-manufacture of these graphene-based digital biosensors is achieved by successfully integrating graphene into standard electronic high-volume production processes. Access to this type of production opens the door for rapid deployment of nanoelectronic sensors outside the research space. The low power and resource usage of these biosensors enables biotech engineers to gain immediate control over precise biological and environmental data.

The prevailing philosophy in biological testing has been to focus on simple tests with easy to interpret information such as ELISA or lateral flow assays. At the same time, there has been a decades long understanding in device physics and nanotechnology that electrical approaches have the potential to drastically improve the quality, speed, and cost of biological testing provided that computational resources are available to analyze the resulting complex data. It is well established in the nanotechnology literature that techniques such as field effect biosensing are capable of rapid and flexible biological testing. Until now, access to this new technology has been limited to academic researchers focused on bioelectronic devices and their collaborators. Here we show that this capability is retained in an industrially manufactured device, opening access to this technology generally.

The world is entering an inflection point in medical and biological testing with the simultaneous emergence of improved testing technology, advanced software tools, and increased expectations for quality healthcare worldwide. Organizations like the Qualcomm Tricorder XPRIZE and Gates Foundation have pushed for integrations of varied technologies in clinical tests to demonstrate potential application [1]. Traditional healthcare companies market point-of-care tools with limited test libraries [2]. In each case, complex, analyte-specific reagents and intricate protocols are essential for multiple platforms and deep biochemical or clinical expertise to replicate the capability of a central lab [3].

There is a need for information-dense single assays that break the mold of expensive labs running colorimetric and PCR-based assays [4]. Label-free measurement tools based on field-effect sensors should lower the amount for most liquid reagents, decrease power requirements, and shrink the size of handheld testing devices [5]. These tools will be capable of performing a wide variety of chemical and biochemical assays built on top of a single sensor manufacturing chain, leading to lower overall cost for biological measurements.

The unique attributes that are required to build effective field effect biosensors are a combination of semiconductor behavior with chemical stability of the sensor surface in air and salt water [6]. Materials like silicon require oxide layers between the transistor channel and the environment, limiting the sensitivity of field effect sensors made using those conventional materials [5]. Materials, such as graphene, carbon nanotubes, and molybdenum disulfide have the unique combination of chemical stability and electric field sensitivity desirable to create sensitive electronic interfaces to biological molecules [7]. This has led to a dense literature covering chemical and biological sensors using these materials [8–20]. Several attempts were made to produce carbon nanotube biosensors for biomedical use in the early part of the twenty-first century with limited results due to manufacturing difficulties [14]. Fabrication techniques using molybdenum disulfide have not matured sufficiently for devices to move beyond the proof of concept stage [15].

2 Principle of Operation

2.1 Overview

With graphene-based biosensors, scientists have direct visibility into the binding interactions that natively occur in biological systems without intermediary translations from optical data. In particular, graphene biosensors using field effect biosensing (FEB) offer a label-free technology for measuring biomolecular interactions. FEB, an electrical technique, measures the current across a graphene biosensor surface functionalized with immobilized biomolecular capture probes (Fig. 1a). Any interaction or binding that occurs on the biosensor surface causes a change in conductance of the biosensor that is monitored in real-time (Fig. 1b), enabling accurate kinetic, affinity, and concentration measurements. These measurements are consistent with other biosensor advancements that aim to achieve label-free detection for biochemical analysis. This includes impedimetric techniques, surface plasmon resonance-based optical detection systems, or mass-sensitive devices, such as surface acoustic wave devices (SAW) [21].

Graphene FEB sensors integrate biologically active materials (i.e., the immobilized capture probe) with graphene-based electronics to detect the binding of an analyte in solution. When analyte binds to the probe, the charge distribution at the surface changes, triggering a change in graphene field effect transistor (gFET) electrical characteristics. This can be obtained by measuring the source and drain current, which effectively converts biological events into electrical signals, such as current. Current (I) changes are directly linked to the analyte concentration, and the concentration of the analyte as well as the kinetic binding data and affinity of the analyte to the target can be detected.

The general concept of biosensing was introduced by Clark in continuous monitoring of chemical composition of blood in cardiovascular surgery as early as 1962 [22]. Additionally, the concept of charge detection, which is the foundational research for graphene FEB, is not new and has been utilized in the insulated-gate field-effect transistor (IGFET) [23] or metal-oxide-semiconductor field-effect transistor (MOSFET) starting from the 1960s [24]. The MOSFET is composed of a silicon substrate that has connections for the source and drain, as well as a layer of silicon dioxide on top. In the typical MOSFET setup, the oxide is coated with a gate metal. When a gate potential is applied, a conducting channel is generated in the silicon, which can be measured as a resistance between the source and drain. Adapting the MOSFET design to operation in liquid for sensing application has been reported by Bergveld in 1970 [25]. The so-called ion-sensitive field effect transistors (ISFETs) are composed of source and drain areas connected by a semiconducting channel of different doping. In ISFETs, the reference electrode (RE) passes no current and utilizes applying the gate voltage while providing a constant potential to the solution. The conductance of the channel is modulated by the potential of the liquid gate. The conducting channel in the semiconductor is separated from the solution by a passivation layer put in place to prevent chemical oxidation of the silicon by water. The concept has been originally developed for ion sensing. Here an ion-selective membrane has been coupled to the gate insulator to allow a defined potential formation in dependence on the respective ion concentration in solution [26].

Later this concept has been extended to biomolecular sensing (BioFET) [25]. Here different principles have been used. In combination with enzymes (ENFET) the detection is based on the production/consumption of an ionic edduct/product (often H+) during the biomolecular conversion which changes the potential at the interface ion-selective membrane/solution and subsequently the source-drain current. This approach is not only valuable for single metabolites but also for measuring cellular activities. [27, 28] One notable commercially successful application of this technology is Ion Torrent, which detects H+ production when nucleotides are incorporated during DNA sequencing [29].

To expand the utilization of BioFETs, approaches were developed where specific biological receptors (or probes) are conjugated on the gate to directly capture the desired analytes based on bioaffinity [30]. The specific binding event is directly transduced, and various BioFETs have been developed for the detection of nucleotides [31–33] and proteins [34–36]. However, it was realized that the charge situation plays an important role and also the ion concentration in solution. The ions in solution can screen part of the charge of the surface attached biomolecule. This can be expressed by the Debye length. This Debye length

screening is proportional to the reciprocal of the square root of the ionic strength and is quite small in physiological solutions, less than 1 nm [37–39]. This has limited the application to mainly highly charged molecules.

On the other hand, organic field-effect transistors (OFETs) represent the next stage of development in transistor technology. OFETs use organic semiconducting materials such as polymers, instead of traditional inorganic materials like silicon. There are several advantages to using organic materials in transistors: (1) Flexibility: Organic materials can be printed on flexible substrates, allowing for the creation of flexible and conformable electronic devices. (2) Low-cost fabrication: Organic materials are less expensive to produce and process than inorganic materials, making them an attractive option for large-scale production. (3) Solution-processability: Organic materials can be dissolved in solvents and processed using solution-based techniques such as inkjet printing, roll-to-roll printing, and spray coating. (4) Tun-ability: The electronic properties of organic materials can be easily tuned by modifying the chemical structure of the material, enabling the creation of a wide range of devices with varying properties. OFETs have several potential applications, including flexible displays, smart sensors, and wearable electronics. Additionally, the use of organic materials in transistors is environmentally friendly, as organic materials are often biodegradable and can be recycled. Overall, the development of OFETs represents a significant advancement in transistor technology and has the potential to revolutionize the field of electronics with its unique advantages.

2.2 gFET FEB Compact Model

In order to illustrate the advantages of graphene-based field effect transistors first the conditions of operation of a silicon based ISFET or BioFET will be described. The presence of bound charged biomolecules at the sensing surface of the transistor will be detected by changes in channel conductance of the FET due to a change in the effective gate potential. The sensing surface in a BioFET consists of the interface between a passivating layer + ion-selective layer, such as silicon nitride, and the solution.

The amount of bound biomolecules changes the charge at the sensor's surface, thus modifying the gate on the transistor. The charge per biomolecule depends upon the biochemistry, with dependence on the pH of the aqueous solution and the biomolecules' isoelectric points [40, 41]. Historically, in commercial ISFET applications, the signal of interest is the shift in threshold voltage V_T from the addition of ΔV_I [26]. but the source-drain current can also be followed resulting in better sensitivities which is shown in the following equation:

$$I_{SD} = \frac{W}{L}\left((V_{GS} - V_T)V_{DS} - 0.5V_{DS}^2\right)\mu_{eff}C_g \tag{1}$$

where W is the width of the channel, L is the length of the channel, V_{GS} is the gate-source voltage, V_{DS} is the drain-source bias, and μ_{eff} is the effective mobility incorporating the effects of finite contact resistance. It should be emphasized that in this equation, the

capacitance of the gate insulator C_g is contained instead of the double layer capacitance C_{DL} which directly influences the source-drain current.

In these silicon devices, the dielectric in between the channel and the liquid introduces not only a small capacitance but may also cause background signal due to the interposing charge traps between the channel and liquid [42, 43]. In gFETs, the channel material is a single atomic layer of carbon in the form of chemical vapor deposition (CVD) grown graphene [44, 45]. This has beneficial electronic and chemical effects for biosensing. The graphene surface is chemically compatible with biological electrolytes, so dielectric passivation layers are not required. This enables direct interaction with the conduction channel via simple functionalization chemistries. In addition, the conductivity of gFETs is extremely sensitive to interactions near the channel because of its two-dimensional structure, as all atoms are surface atoms [46].

Rather than using the source-drain follower measurement scheme commonly used for silicon ISFETS, gFET FEB sensors reported in the literature are usually operated as signal amplifiers, in which the gFET output current response ΔI_D is measured [37, 45, 47–49]. In this case the external operational amplifier (op-amp) which is an integrated circuit for amplifying weak electric signals will be configured as a transimpedance amplifier. Using the typical small signal FET model [45], the change in drain current from a binding event at the surface can be approximated as:

$$\Delta I_D = \frac{W}{L} V_{DS}\, \mu_{eff} \frac{C_{FET}\, \Delta\sigma}{C_{DL} + C_{FET}} \tag{2}$$

where C_{FET} is the field effect transistor capacitance and C_{DL} is the double layer capacitance. In comparing Eqs. 1 and 2, it can be seen that the overall gain is an increase in the current response by a factor equal to the transconductance $g_m = (W/L)V_{DS}\mu_{eff}C_{FET}$. Graphene has high intrinsic carrier mobility ($\mu > 2{,}000\ cm^2\ V\ s^{-1}$) compared with silicon, leading to an advantage over silicon in this amplification mode. This advantage in transconductance is compounded in biosensing applications because of the increased C_{FET} in graphene compared to silicon/insulator structures. This is because C_{FET} is a series combination of all the capacitances between the interface and the channel, which includes the capacitance of the dielectric passivation layer in silicon, which isn't present in graphene. In gFETs C_{FET} can be comparable to C_{DL}, leading to a higher overall gain [50, 51].

Beyond the increase in signal gain and the lower noise due to no charge traps between the channel and the liquid, a gFET's ability to operate in amplification mode with high transconductance devices allows for multimodal sensing. Multimodal sensing involves the integration of multiple sensors or sensing modalities, such as optical, acoustic, and electrical sensors, to provide a more comprehensive and accurate understanding of the environment or system being monitored. For instance, a multimodal biosensor may include electrodes for measuring neuron spikes electrical signal, optical sensors for measuring blood oxygen

levels, and accelerometers for measuring body movement and activity. Changes in the total gate capacitance C_T and changes in the channel mobility μ_{eff} modulate the transconductance and can be detected by sweeping the liquid gate voltage to measure the $I(Vg)$ transfer curves. This requires using both a gate electrode and a reference electrode in a manner similar to how an electrochemical cell uses a counter electrode and a reference electrode to ensures the potential is properly measured while sweeping [52]. This uses a gate circuit design similar to an electrochemical potentiostat, allowing for very accurate and dynamic control of the liquid potential and continuous measurement of the current vs gate voltage transfer curve. From this, features such as the charge neutrality potential, resistance, surface charge density, mobility, and capacitance can all be extracted simultaneously.

Changes in capacitance result from the displacement of charges in the liquid by the presence of the biomolecules, which can change the double layer capacitance of the channel with the liquid gate [45]. In this case, the biomolecules do not need to be necessarily charged to be sensed but sensitivity might be limited. Mobility changes will be stronger in the opposite limit of strongly charged targets, where charges near the channel can scatter charge carriers, thereby decreasing the mobility [37, 49].

The biomolecules in reality will not assemble as uniform layer of charges right at the interface, but rather will sit some distance away from the FET channel. If the biomolecules sit much farther away than the Debye length, the ions in solution will nearly completely screen the charges of the biomolecule, and they will not materially affect the gate potential of the device. Modern gFET biosensor designs mitigate Debye screening by employing the Donnan effect concept from membrane science. As usual in biosensors based on affinity the capture molecules are immobilized in a layer – here on top of the graphene channel. These layers are composed of various types of molecules with different functions, including biological receptor molecules for the analyte of interest, linker molecules if the biological receptor cannot be directly attached, and blocking molecules such as BSA and PEG to passivate the empty linkers and channel. [13, 47–51, 53] As with the analytes of interest, the organic molecules used in the Donnan layer will usually be charged when in buffer solution, depending on their isoelectric point and the local pH. Larger biomolecules cannot generally penetrate the layer, so the layer is mainly permeable for ions (and small molecules). A concentration gradient is formed between the immobile charged molecules within the layer and the mobile ions in the bulk solution, which in turn creates a potential difference between the bulk solution and the immobilized layer. The potential within the layer, the Donnan potential, is sensitive to pH and ionic concentration [54, 55], and this is the potential directly sensed by the FET. The Donnan potential changes as new biomolecules are bound to or released from the layer of biomolecules immobilized on the surface of the gFET.

Adding a Donnan layer to the interface has led to the modern era of biosensor FETs that can operate even in physiologically relevant, high ionic strength buffers [13, 56–59]. The effect enables sensor to be much more sensitive to bound analyte than under a double layer alone, because, in Donnan equilibrium, the double layer is moved away from the surface of the FET and instead forms at the Donnan layer interface [55]. If the biological receptors are captured within the Donnan layer and so beneath the double layer, the screening is much reduced because of the decreased concentration of mobile ions [53]. Capacitance mode

sensing also benefits from the presence of the Donnan layer, as C_{FET} must be modified to include the series capacitance of the Donnan layer, C_{Don}, which will be smaller than the double layer capacitance and can therefore limit the total capacitance. C_{Don} is proportional to the ionic strength and thereby is more sensitive to changes in ionic concentration than the double layer capacitance which is proportional to the square root of the ionic strength. The presence of large biomolecules, even outside the double layer, can cause large shifts in C_{FET} and the transconductance [57]. This requires that C_{Don} is the limiting term in C_{FET}, true for gFETs, but may not be true in silicon BioFETs with passivating layers that themselves limit C_{FET}.

A current model incorporating these concepts is shown in Eq. 3.

$$I \approx \frac{W}{L}\mu\, C_{tot}\, V_{DS}\left(V_{CNP} - V_g + 2.3\ \phi_{th}\alpha\ \Delta pH + \left(1-\alpha\right)\Delta\varphi_D\right) \tag{3}$$

where I is the current, μ is the charge carrier mobility, C_{tot} is the total capacitance per unit area, V_{cnp} is the charge neutrality point (CNP) potential, V_g is the gate voltage, alpha is pH sensitivity factor, ΔpH is the pH shift from the neutral surface, $\Delta\varphi_D$ is the Donnan potential which is explained in Eq. 5, and φ_{th} is the thermal voltage at room temperature. In the context of a liquid gate or pH sensor, the thermal voltage should be thought of as a thermodynamic potential driven by a change in ionic concentration at a surface. It is typically constructed as $R*T/F$ with T being temperature, R being the ideal gas constant and F being Faraday's constant.

This model generally relates the current (I) to typical electrical properties such as the charge carrier mobility (μ), total capacitance per unit area (C_{tot}), width (W) and length (L) of the graphene channel, source-drain voltage applied directly to the graphene (V_{DS}), and the gate voltage (V_g) relative to the charge neutrality point (CNP) potential (V_{CNP}). The CNP voltage here is the gate voltage at which there is a minimum in conduction at neutral pH. The capacitance between the graphene and the liquid, C_g, is a series combination of the graphene quantum capacitance, the double layer capacitance, and the Donnan capacitance. It is important to note that Eq. 3 is only valid for hole conduction and does not account for non-linear gate effects near the CNP voltage. It can be combined with a more complete foundational graphene FET model as in Eq. 4:

$$I_{ds} = \frac{\mu\, W\, V_{DS}}{L}\sqrt{C_{tot}{}^2\left(V_{CNP} - V_g + 2.3\ \phi_{th}\alpha\ \Delta pH + (1-\alpha)\Delta\varphi_D\right)^2 + 4\frac{n_0{}^2}{q^2}} \tag{4}$$

Here n_o represents the charge density of conduction-band, q is the charge density of valence-band, and $\Delta\varphi_D$ is the Donnan potential (see Eq. 5). With appropriate construction of the C_{tot}

term, this model can be used to represent electron and hole conduction regimes, and close to the CNP. This model encompasses effects from the liquid gate, surface chemistry, and biochemistry. The remaining undescribed terms in Eqs. 3 and 4 are corrections to the gate voltage due to the influence of pH changes and the Donnan potential. This model assumes operation of the sensor near room temperature, for an equivalent gate voltage less than the CNP voltage, for source-drain voltages below 1 V, and for a channel length greater than 10 μm.

Electronic sensitivity to pH is typically attributed to proton binding to a gate dielectric. For graphene transistors, there is no gate dielectric, but this form of pH sensitivity has been shown to apply through direct shifts in the apparent Dirac voltage [60, 61]. The surface pH sensitivity factor (α) is a material dependent value. For clean isolated graphene, α is a very low 0.02, but in practice this value is increased by the presence of oxides and nitrides used in device fabrication; α values for practical graphene transistors are around 0.37 [62–64]. This term is combined with the thermal voltage (ϕ_{th}), about 26 mV, and pH shift from a neutral surface (ΔpH) to produce the equivalent gate voltage due to pH. The thermal voltage of 26 mV multiplied by a factor of 2.3 that comes from the use of $\log_{10}$ instead of natural log by pH measurement results in the familiar Nernst limit for pH measurements of 59 mV per unit change in pH.

A Donnan potential ($\Delta\varphi_D$) is created when an ion-permeable layer separates two collections of ions, as shown in Eq. 5.

$$\Delta\varphi_D = \phi_{th} \ln \frac{\left(\sqrt{4{c_s}^2 + {c_x}^2} + c_x\right)}{2c_s} \tag{5}$$

Here c_s stands for the ionic strength of the bulk solution and c_x for captured probe ionic strength. All together, this model provides a relatively simple framework for thinking about how a gFET FEB biosensor works.

2.3 Structure of gFET Sensor

A diagram of a gFET FEB sensor is shown in Fig. 2a, and a top-down microscopy image of the active region of an example gFET FEB biosensor is shown in Fig. 2b. During measurement, a liquid drop is placed onto the circular region defined by the black epoxy shown here. The platinum counter and pseudo-reference electrodes built into the sensor surface control and monitor a voltage in the bulk liquid. A blocking layer and embedded biomolecules such as proteins are immobilized onto 15 graphene channels on the surface. This particular design is intended to lower the possibility that localized mechanical damage, such as from a pipette tip, would completely destroy a sensing channel. There are three sensing channels on the chip, each with five transistors spread around the surface.

Carbon-based and non-carbon-based nanomaterials are two main categories of electronic and electrochemical biosensors. Graphene field-effect transistors (gFETs) use a three-

electrode set up called the source, drain, and gate electrode. gFETs are ion-sensitive and current across graphene channel can be modulated by a liquid gate. While FETs can use any semiconductor material, a higher carrier mobility, and its electrophysical properties make gFETs well suited to biosensing.

gFET sensing is quantified by a transfer curve which is collected as current between sources-drain with respect to the applied gate voltages. The lowest point of the transfer curve is called the Dirac point, or the charge neutrality point (VCNP). While other sensors measure current over time and use electrochemical tags, sensing on gFETs is often in terms of the charge neutrality point, capacitance, transconductivity, and current modulation due to functionalization and biomolecule interaction.

2.4 gFET Sensor Biochemical Interaction Model

gFET FEB sensors are typically used to perform label-free affinity binding assays. It is useful to understand the basics of the biochemical interactions occurring on the graphene surface to understand how to separate measurements of the targeted biochemistry from measurements of background effects or contaminants. While data collected from a real-time, label-free biosensor can be analyzed using several models, the standard approach is to use experiment design so that a first-order chemical interaction can be used to model the data.

The mathematics behind the analysis of label-free biosensor data begins with the 1:1 L model and gets increasingly more detailed as more potential convoluting effects are considered [65]. In its simplest form, the Langmuir model describes the binding of one analyte to one capture molecule to form a complex. Further, all binding sites are assumed to be equal and independent and unaffected by mass transport such as diffusion.

In biochemistry and pharmacology, there are very few reactions that are truly irreversible or truly completely reversible. Analyte molecules are continuously binding and unbinding to the thousands or millions of capture molecules bound to the sensor surface. The often non-equilibrium reaction of capture molecule (M) and analyte (A) can be written as [66]:

$$\mathrm{M+A} \rightleftharpoons \mathrm{MA} \tag{6}$$

where TA is the complex of the capture molecule with bound analyte.

Therefore, the binding rate of the analyte is:

$$\frac{d[\mathrm{MA}]}{dt} = k_{\mathrm{on}}\left[\mathrm{M}\right]\left[\mathrm{A}\right] - k_{\mathrm{off}}\left[\mathrm{MA}\right] \tag{7}$$

where [M] is the unoccupied capture molecule concentration, [A] is the free analyte concentration, [MA] is the concentration of the complex of the capture molecule with bound analyte, k_{on} is the association rate constant, and k_{off} is the dissociation rate constant.

When the system is in equilibrium, the concentrations of capture molecules, analyte, and complex of the capture molecule with bound analyte are no longer time dependent.

$$\frac{d[\mathrm{MA}]}{dt} = k_{\mathrm{on}}\left[\mathrm{M}\right]\left[\mathrm{A}\right] - k_{\mathrm{off}}\left[\mathrm{MA}\right] = 0 \tag{8}$$

Then, K_{D} is defined as such and called the dissociation constant.

$$K_{\mathrm{D}} = \frac{k_{\mathrm{off}}}{k_{\mathrm{on}}} = \left[\mathrm{M}\right]\left[\mathrm{A}\right]/\left[\mathrm{MA}\right] \tag{9}$$

In Eq. 7, the number of analyte molecules in each experiment should be several orders of magnitude higher than the number of capture molecules bound to the sensor surface to avoid needing to take into account mass transport effects. Thus, the concentration [A] can be considered constant throughout association since the number of free molecules remains relatively unchanged. Based on this assumption:

$$\frac{d\theta}{dt} = k_{\mathrm{on}}\left(1-\theta\right)\left[\mathrm{A}\right] - k_{\mathrm{off}} \cdot \theta \tag{10}$$

where θ is the fraction (time-dependent) of occupied probes on the sensor surface.

Solving this differential equation produces the relation:

$$\theta = \left(1 - e^{-k_{\mathrm{obs}} \cdot t}\right) \cdot \theta_{\mathrm{eq}} \tag{11}$$

where θ_{eq} is the fraction of occupied capture probes once the binding reaction has equilibrated, and k_{obs} is the observed binding rate at a given concentration is defined as:

$$k_{\mathrm{obs}} = k_{\mathrm{on}}[\mathrm{A}] + k_{\mathrm{off}} \tag{12}$$

This should be familiar to anyone experienced with conventional label-free sensing systems such as surface plasmon resonance (SPR). Building on the experience from that community, there are some useful guidelines in evaluating biochemical interaction data. One issue is connected to non-specific binding to the sensor surface. Non-specific binding refers to adhesion to the surface or surface chemistry of molecules not targeted by the immobilized capture chemistry. In some cases these are chemical interactions that simply appear as adhesion in the data. The qualitative label of nonspecific binding typically implies a quantitative value for k_{on} of less than 10^5 M^{-1} s^{-1} [67]. To account for this problem

calibration is often performed under defined conditions. However, analyzing nonspecific binding is uncertain because, in a genuine sample, accurate kinetic measurement of unknown molecules adsorbing onto the sensor surface is not possible. To address this issue, a different approach is employed by establishing a reference surface without the recognition element and examining the nonspecific binding that occurs there. As a result, in the context of SPR-style sensing, it becomes possible to assess a differential signal to analyze the specific binding and to calculate the rate constant of the specific binding reaction.

For an on-rate of 10^5 M^{-1} s^{-1} you might require many minutes or even hours to achieve half of the equilibrated response to a 1 nM application of [A]. A “specific binder” typically refers to a biochemical system with k_{on} between 10^5 and 10^7 M^{-1} s^{-1}. This is the domain of biochemistry with binding pockets such as antibodies. Here, you will still require several minutes to achieve half of the equilibrated response to a 1 nM application of [A], and longer time for lower concentrations than 1 nM. Binding rates above this range indicate a steered reaction, where the reaction at the surface is consuming reactants from solution faster than diffusion would normally provide them to the surface. An example of this is a CRISPR complex. Such a reaction is the only case in which a 1 nM application of [A] will achieve at least half the equilibrium response in less than 1 min. These guidelines are presented to help understand how to approach data that shows very fast responses. Very fast label-free sensor responses, including responses on gFETs, are typically due to buffer mismatch, addition of preservatives, or presence of some contamination.

3 Basic Applications

3.1 pH and Salinity

The most basic biochemistry measurements start with detecting changes in pH and salinity. gFET biosensors are sensitive to pH, salinity, and the chemical composition of the buffers applied to them. The exact sensitivity of a gFET sensor depends on its specific design and manufacture, as significant contributions to pH and salinity sensitivity of gFETs come from the substrate on which the graphene is deposited and the processing of the sensor surface prior to use. Examples of some pH and salinity sensing measurements are shown in Fig. 3. The percent change in slope appears to be very high because the slope at “0 salt” or negligible salt is very shallow. Pure DI water is effectively an insulator and the liquid gate will not function well. So in terms of % change, there is a large change because the starting value is quite small. Essentially the “gateablility” of the channel changes in a pronounced way with salt concentration while the (effective) resistance of the channel only changes slightly.

The solutions used in Figs. 2c and 3a are standard 1× phosphate buffered saline (PBS) pH 7.41× PBS has a concentration of 0.01 M phosphate buffer concentration, 0.0027 M potassium chloride, and 137 mM sodium chloride or salt concentration. Varying amounts of 100 mM HCl added to 1× PBS to adjust the pH. The sensors were calibrated in pH 7 solutions for these measurements. The solutions used in Fig. 3b, d are NaCl in deionized water.

3.2 Protein-Protein Interactions

Measuring a protein-protein interaction is arguably the most popular and fundamental use of gFET FEB sensors in literature. Here we show an interaction between a monoclonal antibody against human interleukin-6 (anti-IL6) and recombinant human IL6 (IL6). Reagents were sourced from a commercial ELISA kit. IL6 is a well-known cytokine and biomarker related to inflammation, autoimmune diseases, and late-stage cancers. Anti-IL6 was immobilized on graphene chips with a prepared carboxyl surface and activated via standard carbodiimide chemistry in a process shown in Fig. 3 [68]. This approach to surface chemistry is very common in gFET FEB literature. The ethanolamine step here likely presents a dramatic change as it is a charged small molecule that interacts closely with the graphene channel being applied in a low-salt solution.

Figure 4b, c shows the percent change in current and slope responses for 23 different sensor chips all following the same immobilization protocol with the same anti-IL6 reagent. The relatively small variations from chip to chip highlight the stability and reproducibility of the sensors. The immobilization data shows consistent trends. Addition of EDC and sNHS after calibration always leads to a decrease in current, without a change in transconductance slope. This is expected as the carbodiimide chemistry should change the charge at the surface without adding a large amount of material. Addition of the antibody at 30 min leads to a further decrease in current and a large increase in slope. This change is largely due to switching from the pH 6.0 MES buffer used during carboxyl activation to the pH 7.4 PBS pH buffer used during antibody incubation. This highlights the need to limit buffer changes throughout an assay on a gFET, or to make sure the sensor is calibrated and equilibrated in a new buffer when a change in buffer is required. Addition of PEG-amine after anti-IL6 immobilization leads to a small decrease in current and a small increase in slope. This is consistent with association of PEG to the surface to serve as a blocking layer around immobilized protein. After addition of PEG, a complete layer is formed on the graphene surface, enabling a Donnan effect measurement. Addition of ethanolamine (pH 8.0) quenches any remaining activated carboxyl groups, and causes a large decrease in current and a large increase in slope. Rinsing with PBS (pH 7.4) then raises the current and decreases the slope, although never back to the initial starting position. This repeatable set of chemistry and sensor responses indicates both reproducibility of sensor-to-sensor response as well as a detectable and defined change of the surface chemistry due to the immobilization process. These kinds of evaluations of surface chemistry process and repetition across multiple chips are necessary to be confident in subsequent biochemical measurements.

It has to be emphasized here that such approaches are common for several label-free measuring techniques in order to make sure that observed effects can be correlated to a biomolecular event and not to other effects in solution or on the surface. This is often ignored and thus, erroneous conclusions occur.

The effectiveness of this immobilization process is demonstrated in the sensing measurements shown in Fig. 5. Different concentrations of IL6 in PBS were applied to the anti-IL6 immobilized chips. The different concentrations of IL6 lead to different response magnitudes and different speeds of interaction, as expected for any kinetic binding

measurement. This data compares well with the metrics provided by the ELISA kit from which the reagents were taken and previous IL6 standard curves gathered on graphene FEB sensors [69]. This is an example of the kind of information available in a real time assay that is not possible in an end-point assay. In addition, it highlights how process, user, and chip variation may be manifested in the data.

When running an ELISA with this kit, the expected lower limit of detection is <2 pg mL^{-1}, and the linear range of response is between 7.8 and 500 pg mL^{-1} (FEB range of response is 2 pg/mL to 1,000 pg/mL). Here, we have reproduced the ELISA quality while adding kinetic information. We have removed the need for labels while providing more information-dense real-time data than an end-point assay technique like ELISA.

3.3 Small Molecule Measurement

Building on sensing protein-protein interaction measurements, the same gFET sensor design can be used for protein-small molecule measurement. This type of measurement is particularly useful for pharmaceutical research. Here, we show an example of a rank-ordering experiment. The purpose of this set of measurements is to compare the relative binding affinities of several small molecules to the same protein. When working with small molecules, it is important to perform appropriate controls. Nonspecific binding of small molecules to graphene is extremely common. If a complete concentration vs response curve can be taken, a comparison of the calculated kinetics relative to values obtained from other methods can be a helpful check that nonspecific binding is not dominating the observed response.

In this case, the small molecules SPD304, Evans Blue, and Trypan Blue were investigated as drug compounds interacting with the target protein, Tumor Necrosis Factor alpha (TNFα). The assay buffer for all small molecules composed of 1× PBS (0.01 M phosphate buffer concentration, 0.0027 M potassium chloride, 137 mM sodium chloride, pH 7.4), and multiple concentrations were measured for each small molecule.

Fresh assay buffer was added to the chip with the immobilized protein to calibrate a baseline measurement for 5 min, followed by the addition of the compound in assay buffer for 10 min to measure association. After the association measurement was complete, assay buffer was added to measure dissociation of the interaction. Recall that unlike a pure electrochemical sensor, a properly constructed FEB surface is sensitive to changes in the charges within the immobilized layer through measurement of changes in the Donnan potential. When a small molecule displaces the normal salts and hydrogen bonding network on a protein, there is an overall change in this value.

A dose-response curve of the current measurement is plotted in Fig. 6 as the sensor response versus concentration of the compound as the compound interacts with the target protein TNFα. Affinity ranking is determined from the dose-response curves and the associated kinetic binding data. The affinity ranking is comparable to the rank ordering of the known IC_{50} values: $K_D = 3.3 \pm 0.7$ μM SPD304, $K_D = 1{,}102 \pm 107$ μM Evans Blue, and $K_D = 2{,}454 \pm 415$ μM Trypan Blue compared to $IC_{50} = 22$ μM, 750 μM, and 1,000 μM

respectively [70, 71]. The results show that an important drug discovery measurement, affinity ranking for small molecule biochemistry, can be performed on gFET FEB sensors.

4 Bioaffinity-Based Detection

4.1 DNA and RNA Detection

Perhaps the most important area of active research in gFET biosensors is the detection of DNA and RNA. Affinity-based biosensors for nucleic acid detection can be useful after a sample amplification process such as PCR. An affinity-based biosensor provides little advantage when used in conjunction with sample amplification, and does not address the fundamental limitations of sample amplification. Where gFET sensors provide a unique capability is as a solid-state sensor that incorporates new signal amplification techniques, such as the use of CRISPR. These approaches can match the sensitivity of sample amplification, while avoiding the largest problem of sample amplification, which is the potential amplification of contaminating sequences.

As with some small molecules, nonspecific binding of DNA to the surface of the graphene can affect sensor effectiveness. In addition, when DNA associates with the graphene surface, this interaction can disrupt the hydrogen bonds between complementary DNA strands, decreasing the binding affinity of complimentary DNA strands. Since this is valid for all biosensors with immobilized capture probes, care has to be taken during immobilization.

Even with these complications, a gFET FEB sensor can differentiate target DNA from DNA with even a single nucleotide polymorphism (SNP) in a simple affinity sensor mode using a probe DNA attached to the graphene surface. Single stranded probe DNA attached to the graphene gives a negative V_{CNP} shift after immobilization. When a matching single-stranded DNA molecule is detected, a further negative V_{CNP} shift occurs, while non-matching sequences gave significantly smaller shift in V_{CNP}. This negative shift after target addition should match the shift found when double-stranded DNA is bound to the graphene, indicating that hybridization occurs on probe attached to the graphene [72]. There are reports of gFET affinity binding sensors detecting DNA and RNA at extraordinarily low concentrations. Such results need to be considered in context with theoretical limits of detection based on the expected binding kinetics, measurement time, and diffusion. Using Eqs. 11 and 12 above, it is easy to quickly calculate how long a measurement should take for a particular concentration of DNA.

By bending or crumpling, the graphene layer gFET sensing capabilities can be enhanced due to the changes in the Debye length [73]. In order to evaluate this, a DNA probe has been tethered to both crumpled and flat gFETs and a complementary strand was added to the gFET. Displayed crumpled graphene enhanced the detection of DNA hybridization at LOD of 20 aM, while the flat gFETs displayed a signal change at 2 pM. Additionally, a DNA probe was tethered to the crumbled gFET complementary, to the target miRNA or Let-7b in human serum. While a shift is seen at 20 aM, the standard deviation makes it difficult to differentiate. Another strategy for enhancing sensitivity is using peptide nucleic acid (PNA). PNA is a synthetic oligo, with a peptide backbone in the place of (deoxy)ribose sugar–

phosphate chain. PNAs are more stable and have less negative charge, which improves the probe proximity to the graphene surface. The LOD of DNA concentration using PNA was shown to be 600 zM which is more sensitive than using DNA probes. Crumbled gFETs sensor shows unprecedented and incomparable sensitivity without target amplification. While the results are undebatable impressive, it is important to keep in mind what the resolution of any machine is when examining small shifts, even if the fold change is large. The error of the machine nor signal-to-noise ratio are discussed in the paper, making it difficult to fully assess.

Another way to improve the sensitivity of a gFET sensor for detecting nucleic acids is to use a CRISPR complex to improve the binding and search capabilities of the biochemistry. This can be particularly useful when working with real biological samples that contain small copy numbers of long strands of DNA. This way the novel and ultrasensitive gFET biosensor is combined with the selectivity and specificity of CRISPR-Cas system [47, 74]. Such accurate measurement is specifically useful for the detection of single-point mutation and single-gene disorders such as sickle cell anemia [75, 76] or SARS-Cov2 variants without amplification [74]. This section gives first a comprehensive description about CRISPR-Cas detection system and applications. Then, we will explain the mechanism of CRISPR-Cas gFET detection platforms.

4.2 CRISPR-Cas System

CRISPR (Clustered Regularly Interspaced Short Palindromic Repeats) [77] and associated protein (Cas) has been established as a bacterial immune system [78] evolved in Bacteria and Archaea [79] against bacteriophage invasion. The CRISPR locus has two main parts which when transcribed, become the CRISPR-Cas system. The first part of the CRISPR locus is the Cas operon, which codes for a wide variety of Cas proteins [80]. The Cas protein, or CRISPR-associated protein, is an endonuclease responsible for the binding and cleavage in CRISPR-Cas systems. The other component of the CRISPR locus is the CRISPR array, which contains spacer regions. When transcribed and spliced, these spacer regions become the CRISPR RNA or crRNA, which forms a complex with the Cas protein and guides the endonuclease to the target region of DNA (deoxynucleic acids) or RNA. When the Cas protein and crRNA come together, they form the ribonucleoprotein complex or RNP.

Protospacer Adjacent Motif (PAM), a three to six specific nucleotide sequences (e.g., spCas9, NGG, N can be A/TG/C) is required at the target site to be recognized by the RNP complex to complement with crRNA and cleave the sequence [81].

The trans-activating CRISPR RNA or “tracer RNA,” pairs with the CRISPR RNA (crRNA) to create a functional guide RNA (gRNA). Within this gRNA complex, the tracrRNA acts as a handle for the Cas9 enzyme, while the crRNA spacer sequence guides the complex to a specific viral sequence that matches it. The potential of CRISPR-Cas system to precisely cleave at specific site and easy to engineer guide RNA (=tracerRNA+crRNA) has opened a new frontier in gene editing. For instance, the first pig-to-human heart transplant has been enabled by CRISPR genome editing [82].

In the CRISPR-Cas system, the concept of classes and types is used to categorize and classify different variants of CRISPR systems based on their molecular components and mechanisms of action. Based on the number of subunits in the molecular structure, CRISPR-Cas systems have been divided into two classes, both of which have multiple types and subtypes.

Class I contains types I, III, and IV, made up of multi-subunit complexes [83] These complexes have a broader variety of enzymatic activity including auxiliary messenger molecules, such as cyclic oligoadenylates (cOAs) which can provide additional cleavage events. The most well-known type of Class I is type III which contains Cas10 and a set of auxiliary subunits called Csm and Cmr [84].

Class II contains types II, V, and VI, which only have a single subunit. While 90% of CRISPR systems fall under Class I, they are significantly less well studied than their Class II counterparts, which contain Cas 9 in type II, Cas 12 in type V, and Cas13 in type VI [83]. Because many clinical applications use Class II CRISPR complexes, this is what we will be focusing on for electrical sensing. Cas 9 and guide-RNA (gRNA) complex specifically target and cut dsDNA. However, Class I complexes offer advantages for some applications where the detection of various byproducts can be further utilized for biosensing. For Class II CRISPR complexes, gRNA is made up of two different sections, which can be synthetically produced as a single unit, called the single guide RNA or sgRNA. The crRNA or CRISPR RNA has one segment that is complementary to the target sequence, while the tracrRNA fits into the scaffold of the Cas protein. If both the PAM and target sequence are present, Cas will bind and cut the DNA or RNA.

There are two distinct types of cleavage that Cas can have cis or trans cleavage. Cis cleavage is when the Cas complex cuts at the target region. Trans cleavage, also known as collateral cleavage or non-specific cleavage, occurs during target recognition when the activated RNP complex non-discriminately cleaves either RNA or DNA at off-target sites that partially match the guide sequence of gRNA or crRNA.

Cas9 targets dsDNA and exhibits only cis-cleavage, making it particularly useful for gene editing applications and is also used for CRISPR diagnostic and dead-Cas9-mediated imaging applications. Cas12 recognizes and exhibits cis cleavage on dsDNA and trans-cleavage after target recognition and cleaves ssDNA and Cas 13 targets RNA and displays both cis and trans cleavage [85]. Most of these technologies use Cas9, Cas12, and Cas13 either in isolation or grouped together. However, this field is very much still in its nascence – so more research is conducted about other CRISPR Cas systems, specifically in type I.

4.3 CRISPR-Cas Powered gFET Biosensor

Because of CRISPR-Cas gene editing potential and also for many analytical applications several systems have been described in the literature in combining CRISPR-Cas system with gFET biosensors. Recently, CRISPR Cas13a target detection-mediated collateral cleavage was utilized to detect SARS-CoV2 and respiratory syncytial virus samples without the need for PCR analysis. For instance, functionalized RNA reporter sequence is trans-cleaved upon Cas13a activation by Li et al. gFET platform for amplification-free detection of

SARS-CoV-2 virus [86]. In their platform, a PolyU reporter RNA oligo was tethered to the surface of the gFET. Then, pre-incubated Cas13a and the target RNA were introduced on the gFET. The presence of the target activates the Cas13a trans-cleavage activity towards the PolyU reporter. The sensor monitors the source-drain current before and after adding the target sequences (SARS-CoV-2 N gene, 1 fM) while keeping a constant source-drain voltage (Vds = 100 mV) and sweeping the gate voltage (Vg) from −1 to 1 V with steps of 10 mV. To optimize the sensor response and to decrease the LOD up to 1aM, incubation time, $MgCl_2$ concentration, Cas13a concentration, polyU probe length, and incubation temperature were tested. To further validate the assay design, respiratory syncytial virus (RSV) was also tested and achieved the LOD of 1 aM. The assay was next tested on heat-inactivated SARS-CoV-2 from clinical samples. The assay successfully decimates the difference between positive and negative samples making it comparable to RT-qPCR. The easy programmability of the assay to detect different pathogens displays the robust design of the assay. Since gFETs do not rely on optical sensing, the assays are easily completed by liquid handling devices.

Another successful gFET platform for detecting genetic mutation without DNA amplification developed by Hajian et al. [47] They immobilized CRISPR-Cas9 on gFET to analyze DNA samples collected from in vitro cell lines and clinical samples of DNA with two distinct mutations in patients with Duchenne muscular dystrophy or DMD. In their platform named CRISPR-chip, standard carbodiimide chemistry is used to link dCas9 (catalytically deactivated Cas9) to lattice of the graphene. A scrambled gRNA sequence has been applied in order to access the specificity of the detection. In the clinical investigation, authors demonstrate by targeting exon 51 in the dystrophin gene, the CRISPR-Chip differentiates between healthy and patient samples, DMD patients with a mutated exon 3, and DMD patients with a mutated exon 51. Their results show CRISPR–Chip generated an enhancement in output signal relative to the samples lacking the DNA target sequence without amplification, within 15 min, and with a sensitivity of 1.7 fM.

As shown in Fig. 7, CRISPR-Cas9 protein was conjugated on a gFET surface to detect Sickle cell and Duchenne muscular dystrophy (DMD)-associated mutations at fM concentrations in extracted human DNA without sample amplification [47, 75]. In Fig. 7b, c, it can be observed that CRISPR-Chips functionalized with dRNP-DMD3 and dRNP-DMD51 exhibited a significant increase ($P \leq 0.00059$) in signal output when exposed to genomic samples containing the target exons 3 or 51. This enhancement was observed in comparison to DMD samples that had deletions specifically at exon 3 or 51. Furthermore, additional experiments were conducted to establish a negative signal threshold.

In an additional investigation, Ban et al. have recently developed a single-cell multiomics platform to detect variants of the SARS-Cov2 antigen and viral RNA without amplification [74]. The biosensor platform showcased combines a chimeric probe (RNA-DNA) for detecting RNA using LwaCas13a's collateral cleavage activity. The biosensor has the capability to distinguish unprocessed Saliva samples of SARS-CoV-2, Influenza, and Rhinovirus and a LOD of approximately 65 attomolar (aM) is calculated for viral RNA isolation without the need for amplification.

4.4 Extracellular Vesicles and Cells

In addition to detecting of proteins, small molecules, and nucleic acids as discussed above, gFETs are increasingly being researched for direct detection of cells and extracellular vesicles [87]. For example, exosomes are small extracellular vesicles expelled by both healthy and tumorous cells present in blood serum in high abundance (10^8–10^{11} particles mL^{-1}). The presence of an exosome with cancer-related surface biomarkers and its genetic cargo are important for liquid biopsy diagnostics. By immobilizing anti-CD63 and anti-CD151 antibodies on a graphene channel, a gFET sensor demonstrated specific detection of $CD63^+$ and $CD151^+$ exosomes. The change in electrical properties of the graphene in the presence of highly charged captured exosomes resulted in change in electrical parameters of gFET at low concentrations.

Similar device design and surface chemistry for exosome detection can be extended toward monitoring of interactions with cells. An early example of gFET sensing used a device with an array of graphene sensors to track the flow of cells in a microfluidic channel. In addition to this electrical detection, these sensors were built on top of a glass substrate, which allowed simultaneous optical and electrical interrogation of the cells in the channel. The transparent nature of graphene is often emphasized in sensing literature as beneficial to these kinds of combined optical and electrical measurements. While optical graphene materials and electronic graphene tools are both now much more accessible in biology labs, combined systems remain sophisticated nanotechnology tools. Beyond simple detection of cells, the biocompatible nature of graphene enabled gFET sensors for monitoring cardiomyocytes and neuron activity.

5 Requirements for Successful Use

5.1 Scaled Manufacturing

A major hurdle to providing graphene biosensors to biological researchers is the typical manufacture of nanoelectronics in research-oriented clean rooms by teams of research scientists. Increasingly, there are commercial options for obtaining graphene material, graphene chips, and entire gFET FEB sensing systems.

Critically, the cost of graphene and graphene chips has come down significantly. Figure 8 shows the quality assurance results from an example batch of commercially manufactured gFET FEB sensors. For these chips, the cost of graphene was \$0.019 per cm^2. This comes from the average cost of copper foil of \$0.012 per cm^2 and the cost of power to run furnaces to grow the graphene of \$0.007 per cm^2 of grown graphene. This is less than the price of silicon wafer substrates used for these sensors, which was \$0.40 per cm^2 for 150 mm wafers. The cost of processing the wafers through a commercial foundry was 20-fold greater than the cost of the graphene raw material, making conventional wafer processing the dominant costs in producing a gFET FEB device.

Figure 8 presents quality assurance data from three production lots comprising 27 150 mm wafers and 7,992 chips produced over the course of 1 year. Quality assurance processes focus on reproducibility and cost rather than searching for occasional outstanding performance. Specifically, this means the usage of automated optical microscopy commonly

found associated with commercial silicon fabrication to search for contamination and graphene tearing over entire wafers, rather than using nanotechnology specialized research hardware such as atomic force microscopy or Raman spectroscopy.

Differential interference contrast microscopy is used along with AI-enabled defect identification to perform optical evaluations, such as those shown in Fig. 8b–d. The schematic of the chip side view has been shown in Fig. 2a, b with materials indication. Briefly, yellow material is platinum electrode, blue is the silicon nitride passivation layer, and the line is the graphene electrode.

At the end of the QA process during commercial fabrication, a map of percent yields on different areas of each wafer, shown in Fig. 8e, is produced, and used for chip packaging selection. Although most of the focus for the cost of gFET sensor chips is on wafer scale fabrication issues, the actual driving cost of gFET sensor manufacturing is chip packaging. Costs dominated by packaging are not unique to gFET sensors but are very common across a wide range of electronics. Recently, gFET sensor manufacturers were included in the semiconductor industry working group forming the roadmap for Advanced Packaging. This is the first significant semiconductor roadmap to include graphene chip fabrication which can be found on the Semiconductor Research Corporation Webpage [88].

5.2 Surface Chemistry

When designing your experiment, determining the method of capture molecule immobilization is the first step. Currently, the most common surface chemistries use a pyrene with a butyric acid functional group [89, 90]. This molecule (PBA) can be used as is, or it can be used with an attached N-hydroxysuccinimide ester (PBASE) [91]. Both of these approaches use carbodiimide crosslinker chemistry, but when using PBA, you must apply N-ethyl-N’-(3-dimethylaminopropyl) carbodiimide hydrochloride (EDC) and N-hydroxysulfosuccinimide (sNHS) to activate the carboxylic group immediately prior to use. PBASE does not require this; however, the attached NHS ester will hydrolyze in the presence of water, adding a timing and purity complication to storage and use. Both of these approaches will covalently link to an amine presented by a biomolecule in solution.

Other common surface chemistries include pyrene with a nitrilotriacetic acid (NTA) functional group that will associate with a His tag in the presence of $NiCl_2$, and CLICK chemistry-enabled pyrene linkers. [92]

5.3 Choosing a Capture Molecule for Immobilization

There are many factors to consider when selecting your immobilized capture molecule. First, your target must be able to bind to the graphene biosensor surface. Capture molecule should generally contain a free primary amine to be covalently linked via the common PBA or PBASE chemistries. If this is not the case, more exotic crosslinkers will be necessary. The location of the free primary amine or other binding tag relative to the binding region of the targeted analyte can affect the performance of system as a whole. A binding pocket that is facing down into the graphene will not be effective.

Size also plays an important factor when choosing a recognition element. Smaller immobilized capture probes have reduced interaction surfaces that may be sterically hindered through direct attachment to the surface, and thus obstruct binding to the analyte [93]. For small capture molecules, the use of a spacer arm for attachment to the surface is recommended. The benefit of smaller capture molecules is the proximity of the binding interaction to the graphene surface, which will yield a greater change in electrical properties than when the interaction is further away from the surface (Fig. 9).

Buffer conditions may also affect your choices in recognition elements. Proteins or chemicals in the buffer used during immobilization may interact with your surface chemistry (i.e., bovine serum albumin [BSA] used as a carrier molecule to increase stability of proteins) will also bind along with your specific molecule to the graphene. This can lead to a decrease in signal by reduction in capture probe attachment, or a misleading increase in perceived binding due to your analyte interacting with the nonspecific proteins crosslinked to the surface.

If you suspect that specific capture molecule orientation is crucial, alternative binding strategies may be helpful. For specific orientation of a recognition element to a surface, His-tag mediated immobilization to NTA biosensor chips is often used.

5.4 Capture Molecule in Solution

Several factors should also be considered when selecting your capture molecule. Size of the analyte can affect the amount of measurement time needed, as smaller molecules diffuse much faster than larger molecules. Small molecules may also more easily move through a blocking layer made of a polymer such as PEG. However, large molecules tend to show more clear changes in capacitance due to the increased displacement of liquid volume compared to smaller molecules.

5.5 Buffers and Blocking

gFET sensors are versatile and compatible with many commonly used physiological buffers such as phosphate buffered saline (PBS), N-2-hydroxyethylpiperazine-N-2-ethane sulfonic acid (HEPES), and Dulbecco’s modified Eagle medium (DMEM). Although graphene literature contains many examples of sensing with extremely dilute buffers, variability in measurement will increase with decreasing salt concentration, and gate voltage control is extremely difficult when using less conductive liquids; consider also the stability and function of the biochemistry in addition to the performance of the gFET when choosing the optimum assay buffers. It is also recommended to avoid buffers with pH ≤ 2.0 as extremely low pH can disrupt the pi-pi stacking between commonly used pyrene-based surface chemistries and graphene. The buffers used during EDC/sNHS crosslinking should not include any amine- or carboxylate-containing buffers or components (e.g. Tris–HCl buffer).

As in standard biochemical assays, one goal of blocking is to improve your signal-to-noise ratio by physically blocking nonspecific interactions without interfering with specific binding interactions. An additional goal when using a gFET sensor is to create a Donnan potential at the surface. Polyethylene glycol (PEG) is a common blocker for gFET sensors,

as is BSA. In some cases, adding low concentrations of detergents like Tween 20 to the assay buffers may be more effective than a static blocking layer alone.

Ideally, a gFET FEB sensor is equilibrated and calibrated in a buffer that is as similar as that containing the analyte as possible. This prevents changes in composition such as salt concentration, pH, and preservative concentrations from contributing to the sensor response. For example, if your analyte is in human serum, then you may want to use a synthetic serum substitute as your assay buffer during equilibration, in addition to using it as a diluent. Similarly, for animal samples or cell and tissue lysates, you may want to use a species-specific serum albumin to mimic the nonspecific proteins found in your sample.

5.6 Looking Forward: Multiomics

Almost 20 years ago, the Human Genome Project verified something that greatly complicated the way we understand biology: that proteins are not derived from simple expression of the genetic codes in nucleic acid sequences. The human genome contains open reading frames that code for roughly 20,000 canonical proteins. Around 70,000 additional proteins can be created by using alternative splicing of the DNA code. However, to our best understanding, a single human cell contains at least 1,000,000 different forms of proteins.

The elegance of the Central Dogma of biology that information cannot be transferred from protein to protein has been necessarily augmented by an understanding that reality is much more complicated. The definition and construction of a particular protein is due to multiple overlapping parameters such as gene expression and post-translation modifications, which are regulated by interactions with other genetic molecules, methylation, mutation, and transcription factors. In addition, the function of the same protein requires a multitude of interactions between other proteins, small molecules, and metabolic markers. Complexity in biology comes not only from the complexity of the networks of interactions involved, but also in the variations in the parts of those networks. This compounded complexity creates limits to what can be accomplished via reductionist approaches to biology, as well as limits to the usefulness of naive mappings of engineering and computer science concepts into biology.

This understanding led to the creation of the field of systems biology, the study of emergent patterns from the dynamic complexity of biology rather than focusing on a particular type of molecule, such as genomics, proteomics, or metabolomics. An early editorial in Science put it well: “the pluralism of causes and effects in biological networks is better addressed by observing, through quantitative measures, multiple components simultaneously, and by rigorous data integration with mathematical models.” This powerful concept offers a way forward to understand how observable traits come about in biological systems and the creation of a new approach to measurement: multiomics.

Multiomics is a challenging idea. Gaining understanding of biology at a system level based on combining a large number of simultaneous measurements including pH, mRNA, DNA, and enzyme activity is going to require far more than “simply” fully realizing gFETs as a multiomics measurement platform. There will remain challenges in sample collection and processing, experiment design, data interpretation, and a host of other

issues. Despite all this, “simply” using a single measurement platform to execute a wide range of measurements could open the doors for far more people to try out multiomics studies. To understand and overcome the experimental challenges necessary to standardize and democratize multiomics, we need tools to enable more experimentation, more data, and more creativity. Many of the most popular biosensing platforms have been widely commercially available for decades, and have developmental histories going back 50 years or more. In comparison, gFETs have only recently gained attention as biosensing platform. Yet in that short time, a tremendous amount of progress has been made, demonstrating capabilities far beyond what has been capable with traditional semiconducting materials. The maturation of graphene device manufacturing in recent years shows broad accessibility through scalable commercialization will be realized in near term [45, 68].

In the last few years, we have seen a change in the character of papers published in gFET sensing literature. It is often the case that different fields and different stages of technology development require different types of studies. Classical gFET literature commonly applied a large number of samples to a small number of test chips in a repeated fashion. This was necessary because of the difficulty in constructing a working sensor. Recently, there have been a few studies that follow the statistical conventions of biology research and apply a smaller number of samples to a larger number of test chips. [47, 94–96] This is a subtle but significant difference. Device designs and analysis are standardizing, while gFET production on a small scale is maturing [45, 68, 97].

In the coming few years, we expect to see a transition in proof-of-concept studies using gFETs from testing a single analyte per sample to testing multiple analytes per sample simultaneously. We have seen studies that used hundreds of gFETs, we should soon see the first biosensing studies that use thousands of gFETs. These are small milestones that do not yet reach the scale of multiplexing and throughput that are common with traditional optical methods. The distinguishing characteristic should be that gFETs can monitor protein, small molecule, and genomic activity together at the same time. This, at last, would indicate a transition from “promise” to reality for gFETs as a multiomics platform.

References

1. Chandler BDL (2014) A doctor in the palm of your hand
2. Chin CD, Sia SK (2012) Commercialization of microfluidic point-of-care diagnostic devices. Lab Chip:2118–2134. 10.1039/c2lc21204h [PubMed: 22344520]
3. Bingisser R et al. (2012) Cardiac troponin: a critical review of the case for point-of-care testing in the ED. Am J Emerg Med 30:1639–1649 [PubMed: 22633720]
4. Giljohann DA, Mirkin CA (2009) Drivers of biodiagnostic development. Nature 462:461–464 [PubMed: 19940916]
5. Lowe BM, Sun K, Zeimpekis I, Skylaris CK, Green NG (2017) Field-effect sensors-from pH sensing to biosensing: sensitivity enhancement using streptavidin-biotin as a model system. Analyst 142:4173–4200 [PubMed: 29072718]
6. Bergveld P (1991) A critical evaluation of direct electrical protein detection methods. Biosens Bioelectron 6:55–72 [PubMed: 2049171]
7. Datta SPA (2016) Future healthcare: bioinformatics, nano-sensors, and emerging innovations. In: Nanosensors: theory and applications in industry, healthcare and defense, p 247

8. Ohno Y, Maehashi K, Yamashiro Y, Matsumoto K (2009) Electrolyte-gated graphene field-effect transistors for detecting pH and protein adsorption. Nano Lett 9:3318–3322 [PubMed: 19637913]
9. Lu Y et al. (2012) Graphene-protein bioelectronic devices with wavelength-dependent photoresponse. Appl Phys Lett 100
10. Lerner MB, Dailey J, Goldsmith BR, Brisson D, Charlie Johnson AT (2013) Detecting Lyme disease using antibody-functionalized single-walled carbon nanotube transistors. Biosens Bioelectron 45:163–167 [PubMed: 23475141]
11. Choi Y et al. (2012) Single-molecule lysozyme dynamics monitored by an electronic circuit. Science 335:319–324 [PubMed: 22267809]
12. Cohen-Karni T, Qing Q, Li Q, Fang Y, Lieber CM (2010) Graphene and nanowire transistors for cellular interfaces and electrical recording. Nano Lett 10:1098–1102 [PubMed: 20136098]
13. Gao N et al. (2016) Specific detection of biomolecules in physiological solutions using graphene transistor biosensors. Proc Natl Acad Sci U S A 113:14633–14638 [PubMed: 27930344]
14. Allen BL, Kichambare PD, Star A (2007) Carbon nanotube field-effect-transistor-based biosensors. Adv Mater 19:1439–1451
15. Sarkar D et al. (2014) MoS2field-effect transistor for next-generation label-free biosensors. ACS Nano 8:3992–4003 [PubMed: 24588742]
16. Zuccaro L et al. (2015) Real-time label-free direct electronic monitoring of topoisomerase enzyme binding kinetics on graphene. ACS Nano 9:11166–11176 [PubMed: 26445172]
17. Xu S et al. (2017) Real-time reliable determination of binding kinetics of DNA hybridization using a multi-channel graphene biosensor. Nat Commun 8:1–10 [PubMed: 28232747]
18. Ang PK et al. (2010) A bioelectronic platform using a graphene – lipid bilayer interface. ACS Nano 4:7387–7394 [PubMed: 21067155]
19. Kempaiah R, Chung A, Maheshwari V (2011) Graphene as cellular interface: electromechanical coupling with cells. ACS Nano 5:6025–6031 [PubMed: 21675743]
20. Yang W et al. (2010) Carbon nanomaterials in biosensors: should you use nanotubes or graphene. Angew Chem Int Ed 49:2114–2138
21. Mandal D, Banerjee S (2022) Surface acoustic wave (SAW) sensors: physics, materials, and applications. Sensors 22:820 [PubMed: 35161565]
22. Clark LC Jr, Lyons C (1962) Electrode systems for continuous monitoring in cardiovascular surgery. Ann N Y Acad Sci 102:29–45 [PubMed: 14021529]
23. Janata J, Huber RJ (1980) Chemically sensitive field effect transistors. In: Freiser H (ed) Ionselective electrodes in analytical chemistry. Springer US, pp 107–174. 10.1007/978-1-4684-3776-8_3
24. Sze SM (1981) Semiconductor device development in the 1970s and 1980s – a perspective. Proc IEEE 69:1121–1131
25. Bergveld P (1970) Development of an ion-sensitive solid-state device for neurophysiological measurements. IEEE Trans Biomed Eng BME-17:70–71
26. Bergveld P (2003) Thirty years of ISFETOLOGY: what happened in the past 30 years and what may happen in the next 30 years. Sens Actuators B 88:1–20
27. Milgrew M, Riehle M, DRS C (2005) A large transistor-based sensor array chip for direct extracellular imaging. Sens Actuators B 111–112:347–353
28. Fromherz P, Offenhausser A, Vetter T, Weis J (1991) A neuron-silicon junction: a Retzius cell of the leech on an insulated-gate field-effect transistor. Science 252:1290–1293 [PubMed: 1925540]
29. Rothberg JM et al. (2011) An integrated semiconductor device enabling non-optical genome sequencing. Nature 475:348–352 [PubMed: 21776081]
30. Forsyth R, Devadoss A (2017) Graphene field effect transistors for biomedical applications: current status and future prospects. Diagnostics. 10.3390/diagnostics7030045
31. Estrela P, Stewart A, Yan F, Migliorato P (2005) Field effect detection of biomolecular interactions. Acta Electrochim 50:4995–5000
32. Gonçalves D, Prazeres DMF, Chu V, Conde JP (2008) Detection of DNA and proteins using amorphous silicon ion-sensitive thin-film field effect transistors. Biosens Bioelectron 24:545–551 [PubMed: 18599283]

33. Sakata T, Kamahori M, Miyahara Y (2004) Immobilization of oligonucleotide probes on Si3N4 surface and its application to genetic field effect transistor. Mater Sci Eng C 24:827–832
34. Caras S, Janata J (1980) Field effect transistor sensitive to penicillin. Anal Chem 52:1935–1937
35. Schasfoort RBM, Kooyman RPH, Bergveldb P, Greve J (1990) A new approach to ImmunoFET operation. Biosens Bioelectron 5:103–124 [PubMed: 2331349]
36. Zayats M, Raitman OA, Chegel VI, Kharitonov AB, Willner I (2002) Probing antigen-antibody binding processes by impedance measurements on ion-sensitive field-effect transistor devices and complementary surface plasmon resonance analyses: development of cholera toxin sensors. Anal Chem 74:4763–4773 [PubMed: 12349981]
37. Andoy NM, Filipiak MS, Vetter D, Gutiérrez-Sanz Ó, Tarasov A (2018) Graphene-based electronic immunosensor with femtomolar detection limit in whole serum. Adv Mater Technol 3:1800186
38. Ping J, Johnson ATC (2016) Quantifying the intrinsic surface charge density and charge-transfer resistance of the graphene-solution interface through bias-free low-level charge measurement. Appl Phys Lett 109:1–15
39. Israelachvili J (2011) Intermolecular and surface forces.3rd edn. Academic Press
40. Schasfoort RBM, Bergveld P, Kooyman RPH, Greve J (1990) Possibilities and limitations of direct detection of protein charges by means of an immunological field-effect transistor. Anal Chim Acta 238:323–329
41. Norde W, Lyklema J (1991) Why proteins prefer interfaces. J Biomater Sci Polym Ed 2:183–202 [PubMed: 1854684]
42. Kutovyi Y et al. (2020) Noise suppression beyond the thermal limit with nanotransistor biosensors. Sci Rep 10:12678 [PubMed: 32728030]
43. Liu Y, Georgiou P, Prodromakis T, Constandinou TG, Toumazou C (2011) An extended CMOS ISFET model incorporating the physical design geometry and the effects on performance and offset variation. IEEE Trans Electron Dev 58:4414–4422
44. Lerner MB et al. (2017) Large scale commercial fabrication of high quality graphene-based assays for biomolecule detection. Sens Actuators B 239:1261–1267
45. Goldsmith BR et al. (2019) Digital biosensing by foundry-fabricated graphene sensors. Sci Rep. 10.1038/s41598-019-38700-w
46. Georgakilas V et al. (2016) Noncovalent functionalization of graphene and graphene oxide for energy materials, biosensing, catalytic, and biomedical applications. Chem Rev. 10.1021/acs.chemrev.5b00620
47. Hajian R et al. (2019) Detection of unamplified target genes via CRISPR–Cas9 immobilized on a graphene field-effect transistor. Nat Biomed Eng 3:427–437. 10.1038/s41551-019-0371-x [PubMed: 31097816]
48. Béraud A et al. (2021) Graphene field-effect transistors as bioanalytical sensors: design, operation and performance. Analyst 146:403–428 [PubMed: 33215184]
49. Hinnemo M et al. (2018) Protein sensing beyond the Debye length using graphene field-effect transistors. IEEE Sens J 18:6497–6503
50. Xia J, Chen F, Li J, Tao N (2009) Measurement of the quantum capacitance of graphene. Nat Nanotechnol 4:505–509 [PubMed: 19662012]
51. Mackin C, McVay E, Palacios T (2018) Frequency response of graphene electrolyte-gated field-effect transistors. Sensors 18:494 [PubMed: 29414868]
52. Mannik J, Goldsmith BR, Kane A, Collins PG (2006) Chemically induced conductance switching in carbon nanotube circuits. Phys Rev Lett. 10.1103/PhysRevLett.97.016601
53. Haustein N, Gutiérrez-Sanz Ó, Tarasov A (2019) Analytical model to describe the effect of polyethylene glycol on ionic screening of analyte charges in transistor-based immunosensing. ACS Sens 4:874–882 [PubMed: 30839200]
54. Das S (2014) Explicit interrelationship between Donnan and surface potentials and explicit quantification of capacitance of charged soft interfaces with pH-dependent charge density. Colloids Surf A Physicochem Eng Asp 462:69–74
55. Ohshima H (2009) Theory of electrostatics and electrokinetics of soft particles. Sci Technol Adv Mater 10

56. Gutiérrez-Sanz Ó, Andoy NM, Filipiak MS, Haustein N, Tarasov A (2017) Direct, label-free, and rapid transistor-based immunodetection in whole serum. ACS Sensors 2:1278–1286 [PubMed: 28853283]
57. Palazzo G et al. (2015) Detection beyond Debye's length with an electrolyte-gated organic field-effect transistor. Adv Mater 27:911–916 [PubMed: 25376989]
58. Baldacchini C et al. (2020) A reliable BioFET immunosensor for detection of p53 tumour suppressor in physiological-like environment. Sensors 20:6364 [PubMed: 33171594]
59. Park S et al. (2020) Interfacial charge regulation of protein blocking layers in transistor biosensor for direct measurement in serum. Biosens Bioelectron 147:111737 [PubMed: 31655380]
60. Mackin C, Palacios T (2016) Large-scale sensor systems based on graphene electrolyte-gated field-effect transistors. Analyst. 10.1039/c5an02328a
61. MacKin C et al. (2014) A current-voltage model for graphene electrolyte-gated field-effect transistors. IEEE Trans Electron Dev 61:3971–3977
62. Fu W et al. (2011) Graphene transistors are insensitive to pH changes in solution. Nano Lett 11:3597–3600 [PubMed: 21766793]
63. Wang YY, Burke PJ (2013) A large-area and contamination-free graphene transistor for liquid-gated sensing applications. Appl Phys Lett 103
64. Mailly-Giacchetti B et al. (2013) PH sensing properties of graphene solution-gated field-effect transistors. J Appl Phys 114
65. Hahnefeld C, Drewianka S, Herberg FW (2004) Determination of kinetic data using surface plasmon resonance biosensors. In: Decler J, Reischl U (eds) Molecular diagnosis of infectious diseases. Humana Press, pp 299–320
66. Malmqvist M (1993) Biospecific interaction analysis using biosensor technology. Nature 361:186–187 [PubMed: 7678451]
67. Myszka DG (2000) Kinetic, equilibrium, and thermodynamic analysis of macromolecular interactions with BIACORE. In: Methods in enzymology, vol 323. Academic Press, pp 325–340 [PubMed: 10944758]
68. Lerner MB et al. (2016) Large scale commercial fabrication of high quality graphene-based assays for biomolecule detection. Sens Actuators B. 10.1016/j.snb.2016.09.137
69. Afsahi SJ et al. (2017) Towards novel graphene-enabled diagnostic assays with improved signal-to-noise ratio. MRS Adv:1–7. 10.1557/adv.2017.431
70. He MM et al. (2005) Small-molecule inhibition of TNF-a. Sci Rep 310:1022–1025
71. Song Y, Buchwald P (2015) TNF superfamily protein-protein interactions: feasibility of small-molecule modulation. Curr Drug Targets 16:393–408 [PubMed: 25706111]
72. Manoharan AK, Chinnathambi S, Jayavel R, Hanagata N (2017) Simplified detection of the hybridized DNA using a graphene field effect transistor. Sci Technol Adv Mater 18:43–50 [PubMed: 28179957]
73. Hwang MT et al. (2020) Ultrasensitive detection of nucleic acids using deformed graphene channel field effect biosensors. Nat Commun 11:1543 [PubMed: 32210235]
74. Ban DK et al. (2023) A single multiomics transistor for electronic detection of SARS-Cov2 variants antigen and viral RNA without amplification. Adv Mater Technol 8:2201945
75. Balderston S et al. (2021) Discrimination of single-point mutations in unamplified genomic DNA via Cas9 immobilized on a graphene field-effect transistor. Nat Biomed Eng 5:713–725 [PubMed: 33820980]
76. Lu H-W et al. (2022) The promise of graphene-based transistors for democratizing multiomics studies. Biosens Bioelectron 195:113605 [PubMed: 34537553]
77. Mojica FJ, Ferrer C, Juez G, Rodríguez-Valera F (1995) Long stretches of short tandem repeats are present in the largest replicons of the Archaea Haloferax mediterranei and Haloferax volcanii and could be involved in replicon partitioning. Mol Microbiol 17:85–93 [PubMed: 7476211]
78. Barrangou R et al. (2006) Global analysis of carbohydrate utilization by Lactobacillus acidophilus using cDNA microarrays. Proc Natl Acad Sci 103:3816–3821 [PubMed: 16505367]
79. Barrangou R et al. (2007) CRISPR provides acquired resistance against viruses in prokaryotes. Science 315:1709–1712 [PubMed: 17379808]

80. van der Oost J, Jore MM, Westra ER, Lundgren M, Brouns SJJ (2009) CRISPR-based adaptive and heritable immunity in prokaryotes. Trends Biochem Sci 34:401–407 [PubMed: 19646880]
81. Mojica FJM, Díez-Villaseñor C, García-Martínez J, Almendros C (2009) Short motif sequences determine the targets of the prokaryotic CRISPR defence system. Microbiology (Reading) 155:733–740 [PubMed: 19246744]
82. Reardon S (2022) First pig-to-human heart transplant: what can scientists learn? Nature 601:305–306 [PubMed: 35031782]
83. Makarova KS et al. (2020) Evolutionary classification of CRISPR–Cas systems: a burst of class 2 and derived variants. Nat Rev Microbiol 18:67–83 [PubMed: 31857715]
84. Liu TY, Doudna JA (2020) Chemistry of class 1 CRISPR-Cas effectors: binding, editing, and regulation. J Biol Chem 295:14473–14487 [PubMed: 32817336]
85. Swarts DC, Jinek M (2019) Mechanistic insights into the cis- and trans-acting deoxyribonuclease activities of Cas12a. Mol Cell 73:589–600.e4 [PubMed: 30639240]
86. Li H et al. (2022) Amplification-free detection of SARS-CoV-2 and respiratory syncytial virus using CRISPR Cas13a and graphene field-effect transistors. Angew Chem Int Ed Engl 61: e202203826
87. Hajian R et al. (2021) Rapid and electronic identification and quantification of age-specific circulating exosomes via biologically activated graphene transistors. Adv Biol 5:2000594
88. Zhirnov V MAPT roadmap – SRC. Microelectron Adv Packaging Technol Roadmap. https://www.src.org/about/mapt-roadmap/
89. Zhang X et al. (2013) Application of graphene-pyrenebutyric acid nanocomposite as probe oligonucleotide immobilization platform in a DNA biosensor. Mater Sci Eng C 33:3851–3857
90. Zhu Y et al. (2016) A graphene-based affinity nanosensor for detection of low-charge and low-molecular-weight molecules. Nanoscale 8:5815–5819 [PubMed: 26912374]
91. Wu G, Tang X, Meyyappan M, Lai KWC (2017) Doping effects of surface functionalization on graphene with aromatic molecule and organic solvents. Appl Surf Sci 425:713–721
92. Li H, Papadakis R (2021) Click chemistry enabling covalent and non-covalent modifications of graphene with (poly)saccharides. Polymers 13:142
93. Pollard TD (2010) A guide to simple and informative binding assays. MBoC 21:4061–4067 [PubMed: 21115850]
94. Sandoval JA et al. (2020) Novel mTORC1 inhibitors kill glioblastoma stem cells. Pharmaceuticals 13:419 [PubMed: 33255358]
95. Sadlowski C et al. (2018) Graphene-based biosensor for on-chip detection of bio-orthogonally labeled proteins to identify the circulating biomarkers of aging during heterochronic parabiosis. Lab Chip 18:3230–3238 [PubMed: 30239548]
96. Qvit N, Disatnik M-H, Sho E, Mochly-Rosen D (2016) Selective phosphorylation inhibitor of delta protein kinase C–pyruvate dehydrogenase kinase protein-protein interactions: application for myocardial injury in vivo. J Am Chem Soc 138:7626–7635 [PubMed: 27218445]
97. Ping J, Vishnubhotla R, Vrudhula A, Johnson ATC (2016) Scalable production of high-sensitivity, label-free DNA biosensors based on back-gated graphene field effect transistors. ACS Nano 10:8700–8704 [PubMed: 27532480]

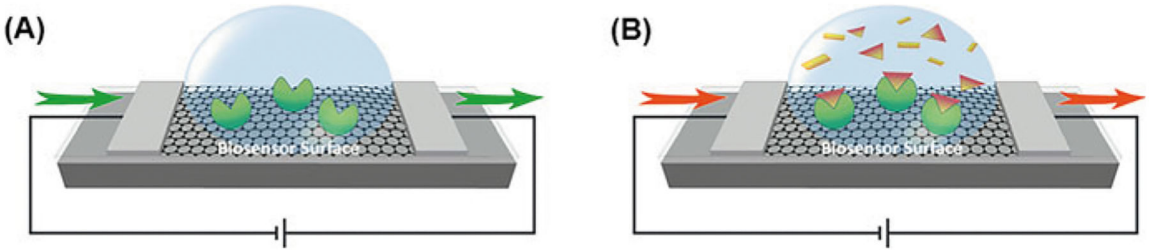

Fig. 1.

A schematic view of the surface of an Agile R100 biosensor chip. (**a**) Immobilized probe bound to biosensor chip. (**b**) Capture probe binding on the biosensor surface detected using FEB and the change in current

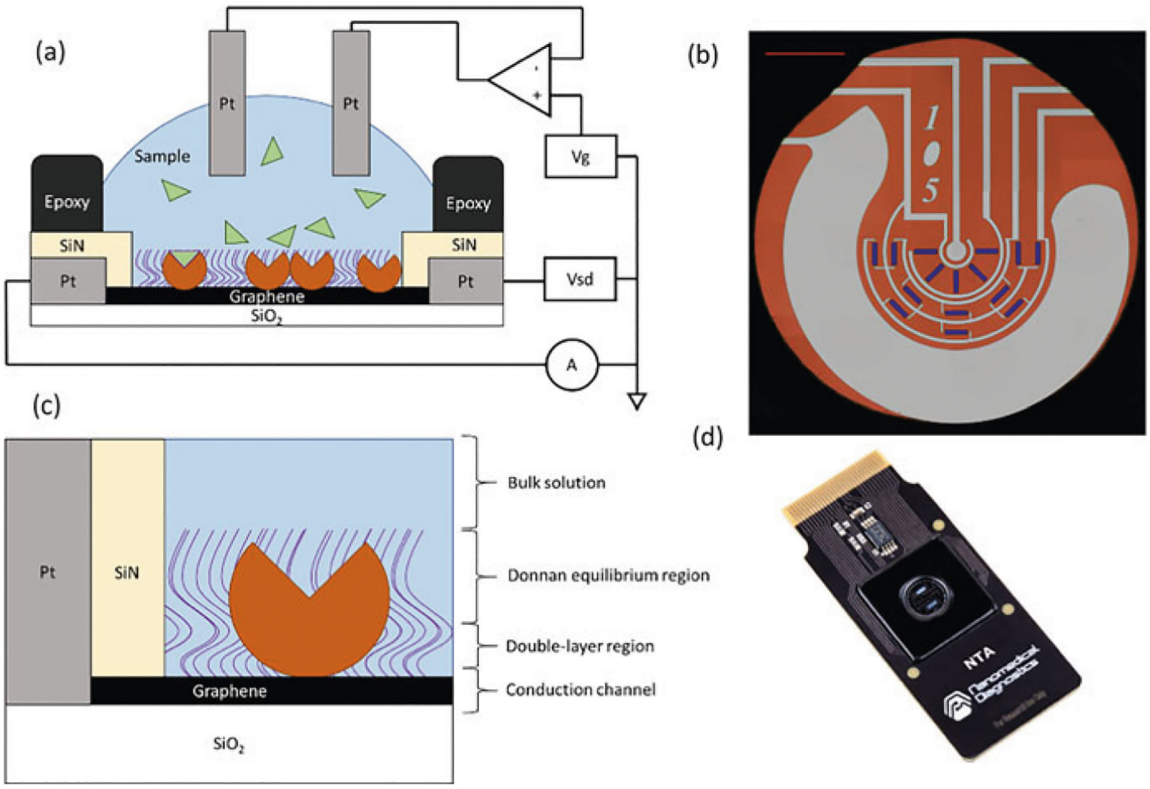

Fig. 2.

(**a**) Scheme of the sensor architecture. Circular sections on top of the graphene represent proteins embedded in a blocking layer, represented by curved lines with two Pt electrodes in the liquid as gate and reference and two Pt electrodes on a chip for source and drain. (**b**) A microscopy image showing an entire sensor surface. Red scalebar is 1 mm. There are 15 graphene strips grouped into three groups of five, exposed through the silicon nitride (SiN = Si3N4) protective layer. The center of the circuit is the gate measurement pad (pseudo-reference) and the large pad surrounding the graphene strips is the liquid gate (counter electrode). (**c**) Diagram of the sensor regions near the graphene. The double layer region is $0.3/\sqrt{c_s}$nm tall, where c_s is the ionic strength of the bulk solution. The Donnan equilibrium region is the thickness of the combined protein and blocking layer on the surface. (**d**) Picture of the complete biosensor

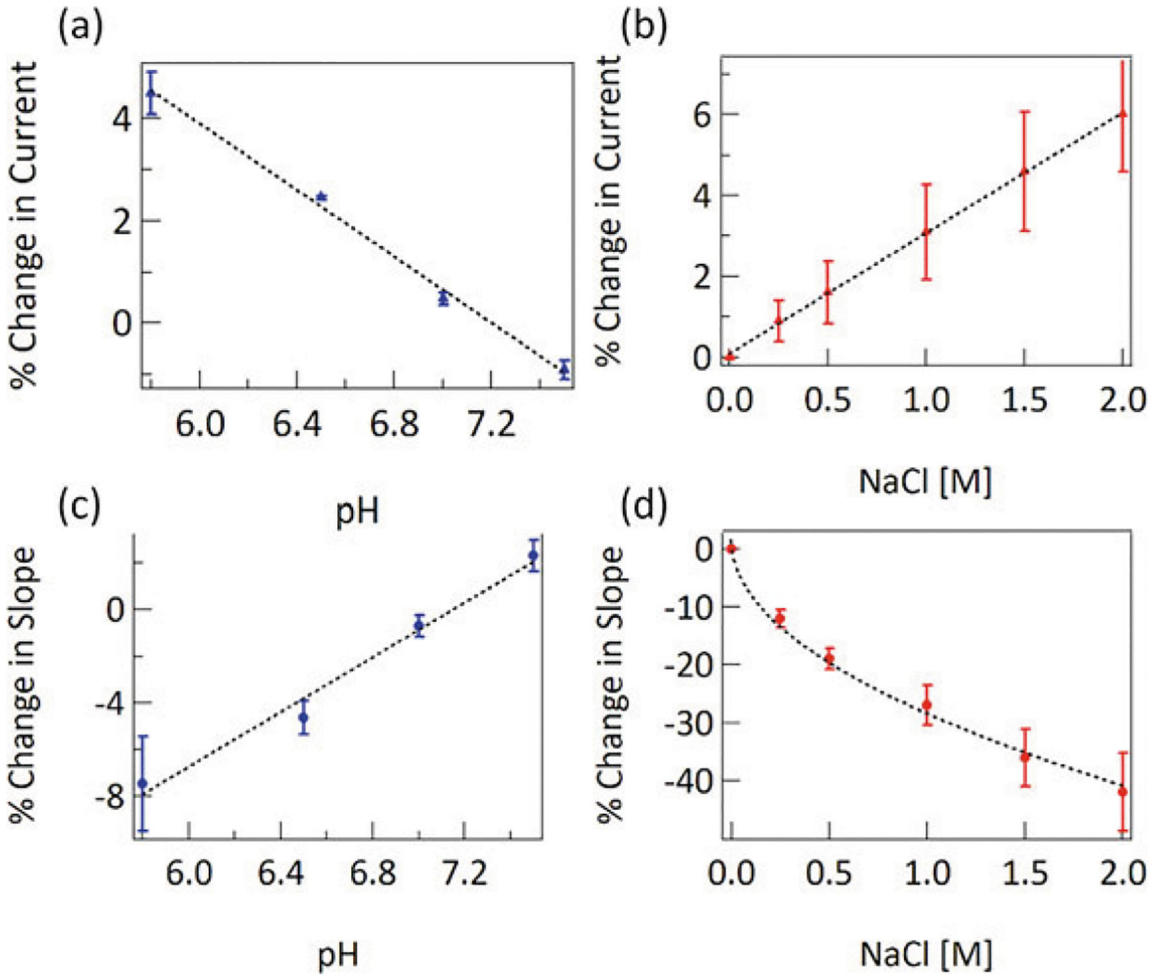

Fig. 3.

(**a**) Change in current due to change in pH. Fit is linear with a slope of −3.2% per pH unit. (**b**) Change in current due to change in ionic strength, when pH is held constant. Fit is linear with a slope of 3.0% per molar unit of NaCl. (**c**) Change in slope (dI/dVg) due to change in pH. Fit is linear with a slope of 5.9% per pH unit. (**d**) Change in slope due to change in ionic strength. Response is fit to $-0.3\sqrt{[\mathrm{NaCl}]}$. Each datapoint in this figure is an average of data from four sensor chips

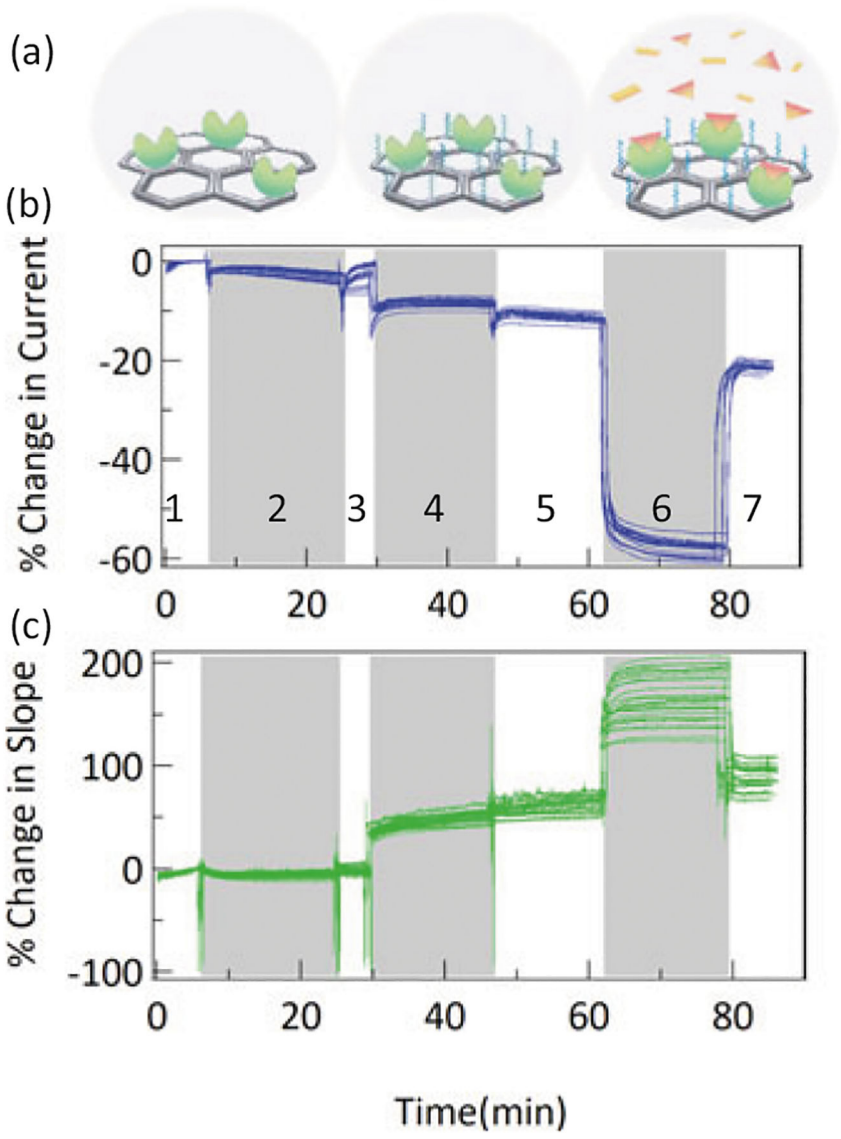

Fig. 4.

(**a**) Diagram of the steps of protein immobilization and measurement used here. First, antibodies against IL-6 are immobilized, then PEG is added as a blocker for nonspecific binding, then measurements are performed with IL-6. (**b**) Change in current and (**c**) change in slope (transconductance) for 23 different sensors during immobilization process. Shading is used to delineate steps: 1: calibration in MES buffer, 2: COOH activation by EDC/sNHS incubation in MES buffer, 3: wash in MES, 4: antibody incubation in PBS, 5: PEG incubation in PBS, 6: reaction of remaining COOH groups with ethanolamine, 7: wash in PBS buffer

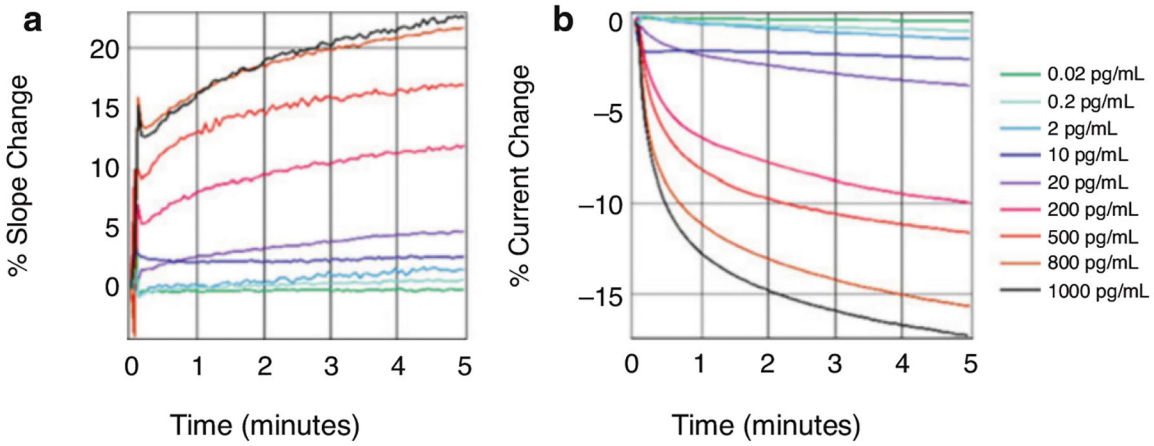

Fig. 5.

(**a**) Change in transconductance of sensors functionalized with antibodies against IL-6 to different concentrations of IL6, each measurement from a different sensor chip. (**b**) Simultaneously measured change in current

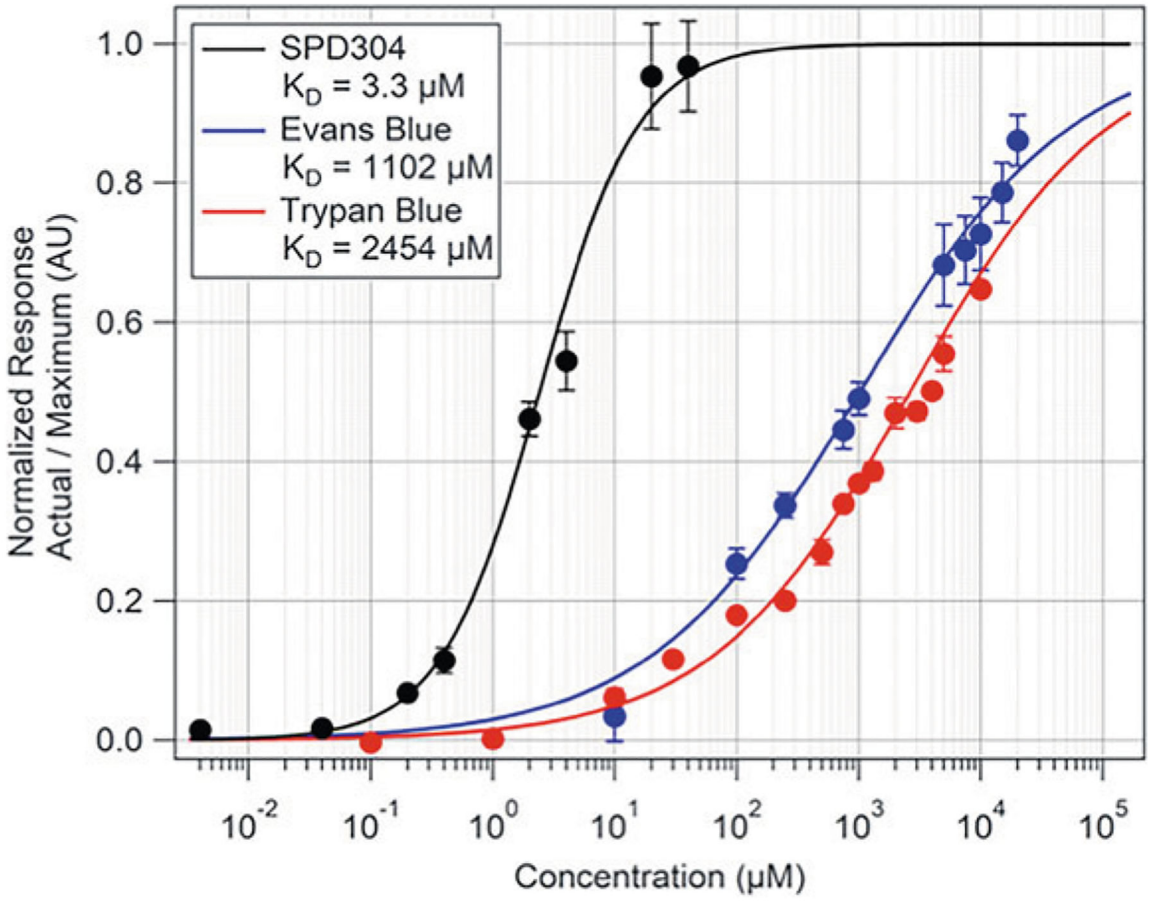

Fig. 6.

Dose-response curves generated for TNFα interacting with SPD304 (black; $K_D = 3.3 \pm 0.7 \mu M$), Evans Blue (blue; $K_D = 1{,}102 \pm 107 \mu M$), and Trypan Blue (red; $K_D = 2{,}454 \pm 415 \mu M$). The determined KD values are given in the legend. For comparison: The IC_{50} of each inhibitor respectively is 22 μM, 750 μM, and 1,000 μM [1]

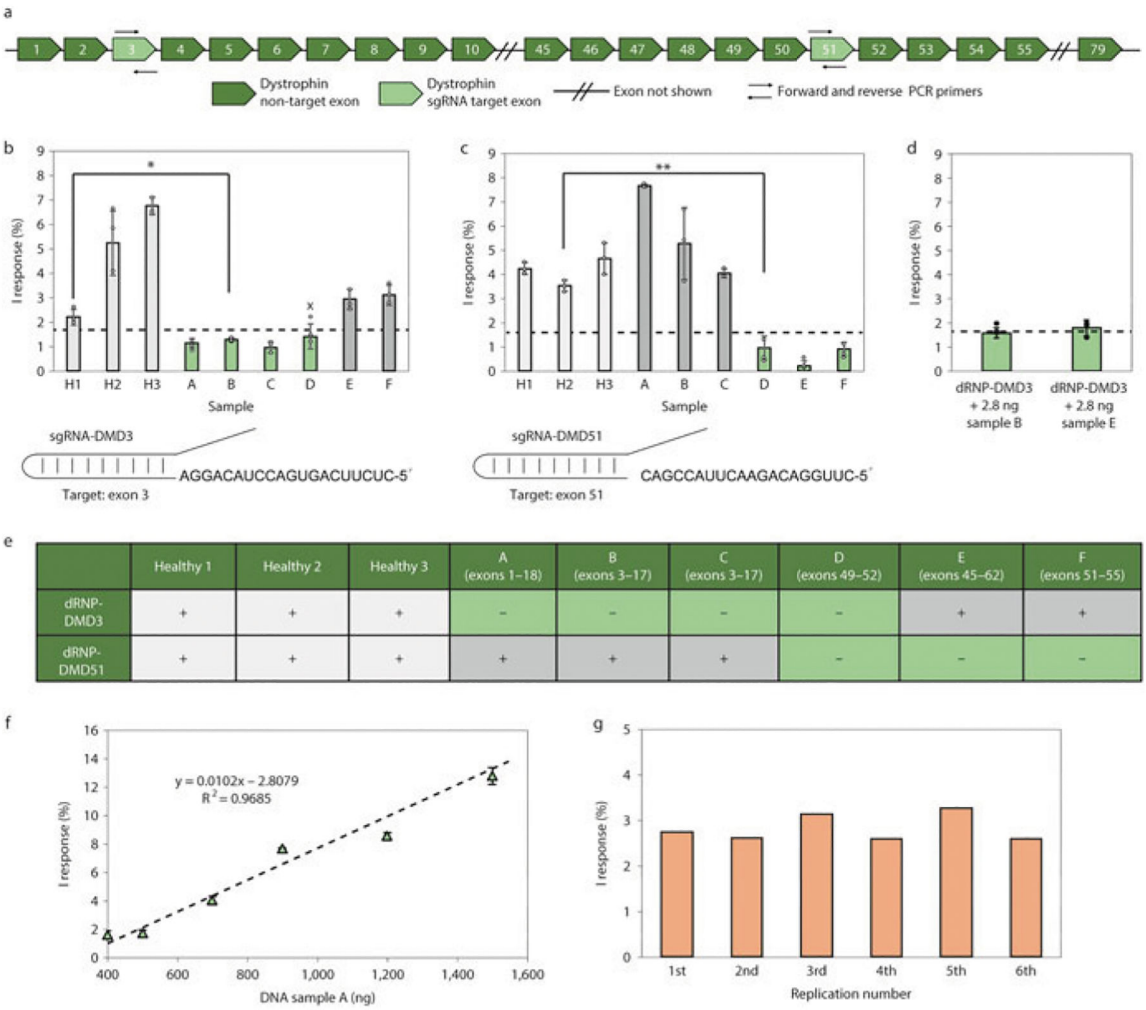

Fig. 7.

CRISPR-Chip analysis of healthy and DMD clinical samples for DMD-associated dystrophin exon deletions. (**a**) Schematic of the dystrophin gene with highlighted target exons. (**b**) Top, I response obtained by CRISPR–Chip functionalized with dRNP-DMD3 in the presence of healthy (H1, H2, and H3) and A-F DMD clinical samples (* $P = 0.017$, one-tailed t-test). Bottom, schematic of sgRNA-DMD3, designed to target exon 3. x represents a false negative as confirmed by sequencing. (**c**) Top, I response obtained by CRISPR–Chip functionalized with dRNP-DMD51 in the presence of healthy (H1-H3) and DMD clinical samples, A-F, (** $P = 0.0014$, one-tailed t-test). Bottom, schematic of sgRNA-DMD51, designed to target exon 51. Samples H1-H3 did not lack any Exon in their dystrophin gene. Samples A, B and C were lacking multiple exons including exon 3 as indicated in table e. Sample D, E and F were also lacking multiple exons including exon 51 as indicated in table (**e, d**) CRISPR-Chip's negative signal threshold was defined by testing CRISPR–Chips with samples lacking target exons at the highest concentrations of genomic sample obtainable from commercially available buccal swabbing methods to ensure that high sample concentrations would not lead to false positives. (**e**) CRISPR–Chip results for the presence of targeted exons (+) within healthy and DMD clinical samples, as defined

by a threshold of 1.73%. (**f**) dRNP-DMD51-functionalized CRISPR–Chip's I response in the presence of varied amounts of clinical sample A (mean; $n = 3$). (**g**) Reproducibility of individual CRISPR–Chips functionalized with dRNP-DMD51 in the presence of clinical sample A. Error bars represent s.d.

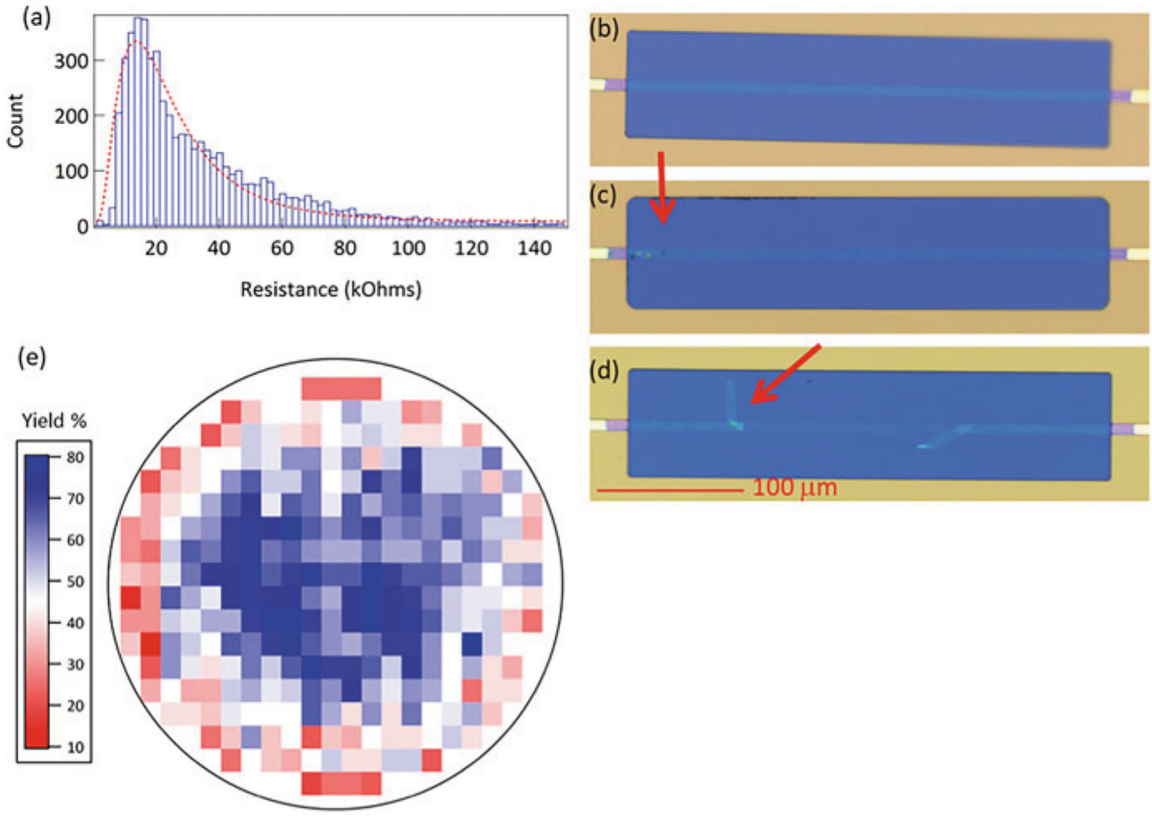

Fig. 8.

(**a**) Histogram of test resistances from 5,543 chips. Fit is a log-normal distribution with a peak at 13.6 kΩ and a standard deviation of 9.2 kΩ. This is for a target graphene resistance of 10 kΩ. (**b**) Microscopy image of defect-free graphene sensor (**c**) Microscopy image of a graphene sensor with minor polymer contamination highlighted by the red arrow. (**d**) Microscopy image of a graphene sensor with major graphene tearing highlighted by the red arrow. (**e**) Wafer yield map combining data from 27 wafers, showing cumulative % yield per 0.4 cm^2 area

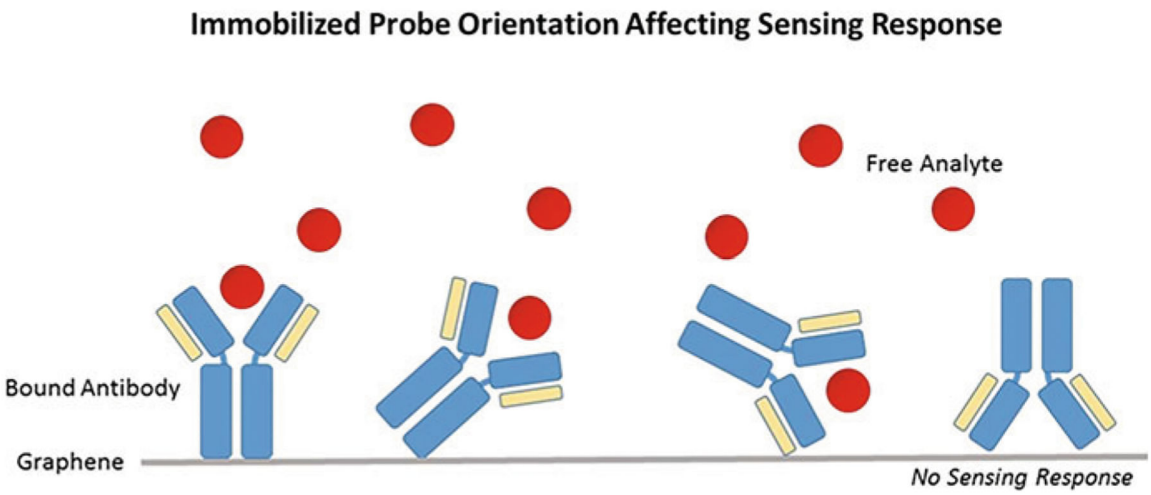

Fig. 9.

Orientation of the capture molecule during crosslinking to the surface of a COOH or NHS biosensor chips is a random event. As shown in figure 9, sensing of the analyte by an antibody is only prevented when the variable region of the antibody binds directly to the surface. This is valid for every biosensor construction